Research Square

Preprints are preliminary reports that have not undergone peer review.
They should not be considered conclusive, used to inform clinical practice,
or referenced by the media as validated information.

Identification of a novel Aβ(pGlu3-x) targeting pathway in Alzheimer's disease

Steffen Roßner

Steffen.Rossner@medizin.uni-leipzig.de

University of Leipzig

Sarah Schrempel

Paul Flechsig Institute - Centre of Neuropathology and Brain Research, University of Leipzig, 04103 Leipzig, Germany https://orcid.org/0009-0003-2436-2866

Corinna Höfling

Paul Flechsig Institute - Centre of Neuropathology and Brain Research, University of Leipzig, 04103 Leipzig, Germany https://orcid.org/0009-0008-6527-6485

Charlotte Minister

Paul Flechsig Institute - Centre of Neuropathology and Brain Research, University of Leipzig, 04103 Leipzig, Germany

Thomas Liepold

Max Planck Institute for Multidisciplinary Sciences, Department of Molecular Neurobiology, Neuroproteomics Group, 37075 Göttingen, Germany

Marcel Naumann

Fraunhofer Institute for Cell Therapy and Immunology, Department of Molecular Drug Design and Target Validation, 06120 Halle (Saale), Germany

Anna Kottwitz

Fraunhofer Institute for Cell Therapy and Immunology, Department of Molecular Drug Design and Target Validation, 06120 Halle (Saale), Germany

Matti Schau

Paul Flechsig Institute - Centre of Neuropathology and Brain Research, University of Leipzig, 04103 Leipzig, Germany

Merle Fricke

Department of Psychiatry and Psychotherapy, University Medical Center Göttingen, Georg-August-University, 37075 Göttingen, Germany

Maike Hartlage-Rübsamen

Paul Flechsig Institute - Centre of Neuropathology and Brain Research, University of Leipzig, 04103 Leipzig, Germany

Max Holzer

University of Leipzig https://orcid.org/0000-0003-1754-9932

David Amschl
Scantox Neuro GmbH, 8074 Grambach, Austria
Roland Rabl
Scantox Neuro GmbH, 8074 Grambach, Austria
Manuela Prokesch
Scantox Neuro GmbH, 8074 Grambach, Austria
Anja Schulze
Fraunhofer Institute for Cell Therapy and Immunology, Department of Molecular Drug Design and Target Validation, 06120 Halle (Saale), Germany
Holger Cynis
Fraunhofer Institute for Cell Therapy and Immunology https://orcid.org/0000-0001-6655-7539
Geidy Serrano
Banner Sun Health Research Institute
Thomas Beach
Banner Sun Health Research Institute
Jorge Ghiso
Department of Pathology, New York University Grossman School of Medicine
Markus Morawski
Paul Flechsig Institute - Centre of Neuropathology and Brain Research
Jens Stieler
University of Leipzig, Paul-Flechsig-Institute of Brain Research
Olaf Jahn
Max Planck Institute for Multidisciplinary Sciences https://orcid.org/0000-0002-3397-8924
Oliver Wirths
University Medical Center, Georg-August University, https://orcid.org/0000-0002-4115-0334
Stephan Schilling
Fraunhofer Institute for Cell Therapy and Immunology, Department of Molecular Drug Design and Target Validation, 06120 Halle (Saale), Germany

---

Article

Keywords:

Posted Date: March 3rd, 2026

DOI: https://doi.org/10.21203/rs.3.rs-8850276/v1

License: This work is licensed under a Creative Commons Attribution 4.0 International License.
Read Full License

Additional Declarations: There is **NO** Competing Interest.

Identification of a novel Aβ(pGlu3-x) targeting pathway in Alzheimer's disease

Sarah Schrempel[1], Corinna Höfling[1], Charlotte Minister[1], Thomas Liepold[2], Marcel Naumann[3], Anna Katharina Kottwitz[3,4], Matti Schau[1], Merle Fricke[5], Maike Hartlage-Rübsamen[1], Max Holzer[1], David Amschl[6], Roland Rabl[6], Manuela Prokesch[6], Anja Schulze[3,4], Holger Cynis[3,7], Geidy E. Serrano[8], Thomas G. Beach[8], Jorge Ghiso[9], Markus Morawski[1], Jens Stieler[1], Olaf Jahn[2,5], Oliver Wirths[5], Stephan Schilling[3,4], Steffen Roßner[1*]

1 Paul Flechsig Institute - Centre of Neuropathology and Brain Research, University of Leipzig, 04103 Leipzig, Germany
2 Max Planck Institute for Multidisciplinary Sciences, Department of Molecular Neurobiology, Neuroproteomics Group, 37075 Göttingen, Germany
3 Fraunhofer Institute for Cell Therapy and Immunology, Department of Molecular Drug Design and Target Validation, 06120 Halle (Saale), Germany
4 Faculty of Applied Biosciences and Process Engineering, Anhalt University of Applied Sciences, 06366 Köthen, Germany
5 Department of Psychiatry and Psychotherapy, University Medical Center Göttingen, Georg-August-University, 37075 Göttingen, Germany
6 Scantox Neuro GmbH, 8074 Grambach, Austria
7 Junior Research Group, Immunomodulation in Pathophysiological Processes, Faculty of Medicine, Martin Luther University Halle-Wittenberg, 06120, Halle, Germany
8 Civin Laboratory for Neuropathology, Brain and Body Donation Program, Banner Sun Health Research Institute, Sun City, AZ 85351, USA
9 Department of Pathology, New York University School of Medicine, New York, NY, USA

Submitted to: Nature Neuroscience

*** Corresponding author:**
Steffen Roßner
Paul Flechsig Institute - Centre of Neuropathology and Brain Research
Liebigstraße 19
04103 Leipzig
GERMANY
Phone: +49-341-9725758
Email: steffen.rossner@medizin.uni-leipzig.de

Acknowledgements
This work was supported by the German Research Foundation (DFG grants #RO 2226/15-1 to SR, #SCHI 1437/2-1 to StS and #WI 3472/11-1 to OW). SaS received a PhD student fellowship awarded by the Federal State of Saxony, MF is an associated student of GRK 2824 - Project number 465640801 funded by the German Research Foundation. We thank Benjamin Hietel (Fraunhofer IZI-MWT), Gabriele Paetzold (MPI-NAT), Renate Jendrek and Isabel Hilbrich (Paul Flechsig Institute - Centre of Neuropathology and Brain Research) for excellent technical assistance. We are grateful to the Arizona Study of Aging and Neurodegenerative Disorders and Brain and Body Donation Program for the provision of human brain tissue. The Program has been supported by the National Institute of Neurological Disorders and Stroke (U24 NS072026, National Brain and Tissue Resource for Parkinson's Disease and Related Disorders), the National Institute on Aging (P30AG019610 and P30AG072980, Arizona Alzheimer's Disease Core Center), the Arizona Department of Health Services (contract

211002, Arizona Alzheimer's Research Center), the Arizona Biomedical Research Commission (contracts 4001, 0011, 05-901 and 1001 to the Arizona Parkinson's Disease Consortium) and the Michael J. Fox Foundation for Parkinson's Research.

Abstract

The pyroglutamate-3-modified form of the amyloid-β (Aβ) peptide (Aβ(pGlu3-x)) is enriched in brains of Alzheimer's disease (AD) patients and is highly neurotoxic, aggregation-prone, resistant to proteolytic degradation and acts as a seed for the co-aggregation of unmodified Aβ. Therefore, it became a pharmacologic target for AD therapy either by inhibition of its synthesizing enzyme, glutaminyl cyclase, or by passive immunization with antibodies targeting the Aβ(pGlu3-x) neoepitope. Here, we present a novel, antibody-independent approach targeting existing Aβ(pGlu3-x) by proteolytic degradation with the physiological enzyme pyroglutamyl-peptidase 1 (PGP-1). We demonstrate degradation of Aβ(pGlu3-x) in *post mortem* brain sections of transgenic mice and AD subjects, along with increased formation of Aβ(4-x). The resulting Aβ(4-x), generated after removal of the pGlu-blocking group, displays slower aggregation kinetics and improved proteolytic degradation by aminopeptidases. In a transgenic mouse model of AD, intracortical PGP-1 injection reduced the Aβ(pGlu3-x) load. Our results strongly support the exploration of *in vivo* PGP-1 delivery routes for therapeutic targeting of Aβ(pGlu3-x) in AD and of other pGlu-modified pathogenic peptides in different neurodegenerative diseases.

Introduction

Amyloid-β (Aβ) pathology is a pathological feature in brains of Alzheimer's disease (AD) patients and Aβ-lowering strategies are considered therapeutic options for AD treatment [1,2]. Aβ is a physiological peptide that is normally cleared by multiple peptidases, including neprilysin (neutral endopeptidase, NEP) [3–5] and insulin-degrading enzyme (IDE) [6,7]. Mutations within the Aβ sequence favor its aggregation [8,9] and Aβ post-translational modifications (PTMs) enhance its aggregation propensity and impair degradation by proteases to promote Aβ pathology [10–12]. Among those PTMs, the pyroglutamate (pGlu)-modified Aβ (Aβ(pGlu3-x)) received increasing attention over the last decades. The Aβ(pGlu3-x) variant was found to be enriched in AD brains [13,14] and was subsequently shown to be resistant to proteolytic degradation [15–17], to act as a seed for aggregation and for co-aggregation of unmodified Aβ [18] and to propagate its structural and neurotoxic properties in a prion-like manner [19].

The generation of Aβ(pGlu3-x) from N-terminally truncated Aβ is catalyzed by glutaminyl cyclase (QC) [20,21]. In human AD brain and in brains of transgenic mice with Aβ pathology, Aβ(pGlu3-x) and QC are present and co-localized in hippocampus [22,23] and neocortex [24]. Based on the pathological Aβ(pGlu3-x) characteristics, it is considered a specific pharmacologic target for AD therapy [13,25,26] and two different strategies were investigated in preclinical and clinical studies.

First, inhibition of QC activity has been considered to prevent pathological Aβ(pGlu3-x) seed formation (**Fig. 1a**). Indeed, pharmacologic inhibition [21,27] and genetic ablation of QC in experimental AD mouse models [22,28] reduced Aβ(pGlu3-x) generation and total Aβ load and ameliorated learning and memory deficits when initiated prior to Aβ(pGlu3-x) aggregate formation. In clinical settings, the safety and tolerability of the QC inhibitor PQ912 (Varoglutamstat) was demonstrated in human subjects [29] and positive effects in neuropsychological testing as well as on synaptic toxicity and neuroinflammation were reported in the phase 2a SAPHIR clinical trial [30]. However, Varoglutamstat treatment missed its primary and secondary endpoints in a phase 2b clinical trial (VIVIAD) [31].

Second, existing Aβ(pGlu3-x) can be cleared from the brain by passive immunization targeting this particular Aβ variant (**Fig. 1a**). Preclinical data on the applicability of this procedure in transgenic mouse models demonstrated the reduction in Aβ(pGlu3-x) and total Aβ plaque load and improvements in cognition [32–34]. In the TRAILBLAZER trials with Donanemab, reductions of Aβ plaque load and decelerated cognitive decline were demonstrated in AD patients leading to approval of Kisunla, e.g., in the USA and the EU [35–37].

While both Aβ(pGlu3-x)-targeting strategies are of high therapeutic potential, there are also limitations. **Prevention of Aβ(pGlu3-x) seed formation** by QC inhibition likely has to be initiated at the earliest preclinical stages possible. Results from transgenic animal studies suggest that the pathological cascade cannot be halted by QC inhibition, if proteopathic

Aβ(pGlu3-x) seeds are already abundant [21]. **Removal of existing Aβ(pGlu3-x)** can be achieved by passive immunization with Donanemab (Kisunla), but this therapeutic strategy is expensive and associated with frequent and sometimes severe amyloid-related imaging abnormalities (ARIAs), such as edema and microbleeds [38,39]. Therefore, we here present an **alternative, antibody-independent approach** that enzymatically targets existing Aβ(pGlu3-x).

While the list of Aβ-degrading enzymes is long [40,41], there is, to the best of our knowledge, no report available that suggests pyroglutamyl-peptidase (PGP) in the context of therapeutic Aβ(pGlu3-x) degradation. There are two types of PGP described in the literature, both of them releasing N-terminal pGlu from a pGlu-modified peptide. Type I PGP is characterized by a broad substrate spectrum (PGP-1, EC 3.4.19.3) while type II has a high selectivity for pGlu-TRH (thyroliberinase, TRH-DE, PGP-2, EC 3.4.19.6) [42,43]. We hypothesize that PGP-1 can degrade Aβ(pGlu3-x) and clear existing Aβ(pGlu3-x)-containing aggregates in brain in an antibody-independent manner (**Fig. 1a**).

Results

Mass spectrometric analyses of Aβ(pGlu3-x) peptide degradation by PGP-1

First, we investigated a potential Aβ(pGlu3-x) cleavage by PGP-1 and PGP-2 at a low level of complexity by using a synthetic Aβ(pGlu3-24) peptide and recombinant PGP enzymes. Incubation of Aβ(pGlu3-24) with the enzymes followed by mass spectrometric analyses showed instant pGlu removal and formation of Aβ(4-24) by PGP-1 (**Fig. 1b**), but not by PGP-2 (**Extended Data Fig. 1a**). In contrast, the Aβ-degrading enzymes NEP and IDE left the N-terminus of the Aβ(pGlu3-24) peptide intact but induced C-terminal truncations. The most prominent cleavage sites for NEP were situated between amino acids Gly-9 and Tyr-10 and between Lys-16 and Leu-17 of the synthetic peptide (**Extended Data Fig. 1a** and **Extended Data Table 1**). The protease IDE generated even more cleavage products, namely between amino acids His-13 and His-14, between His-14 and Gln-15 and between Phe19 and Phe-20 (**Extended Data Fig. 1a** and **Extended Data Table 1**). Thus, of the Aβ-degrading enzymes tested, only PGP-1 is able to remove the N-terminal pGlu blocking group from Aβ(pGlu3-24). When the proteases NEP or IDE were used in combination with PGP-1 for Aβ(pGlu3-24) digestion, an initial formation of Aβ(4-x) generated by PGP-1 was observed (**Extended Data Fig. 1b**), which was subsequently degraded into multiple cleavage products as specified in **Extended Data Table 1**.

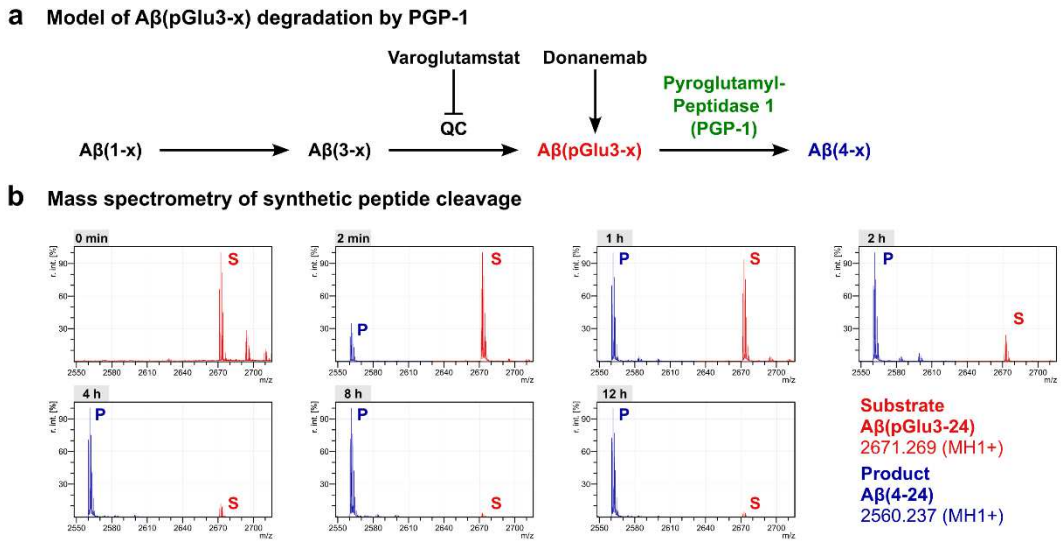


Fig. 1: Enzymatic characteristics of Aβ(pGlu3-x) degradation by PGP-1. a) Hypothetical model of Aβ(pGlu3-x) degradation by PGP-1 resulting in the formation of Aβ(4-x). This approach complements existing strategies targeting the formation of Aβ(pGlu3-x) by QC inhibition with Varoglutamstat and removing existing Aβ(pGlu3-x) by passive immunization with Donanemab, respectively. **b)** Time-dependent removal of pGlu from the synthetic Aβ(pGlu3-24) peptide by incubation with PGP-1 monitored by mass spectrometric analysis for different periods of time as indicated. An initial Aβ(4-24) reaction product is already detectable after 2 min of incubation and Aβ(pGlu3-24) is completely degraded after 8 h.

Characterization of the enzymatic degradation of Aβ(pGlu3-x) deposits by PGP-1 in brain sections of transgenic mice

In order to establish the enzymatic characteristics of PGP-1 towards Aβ(pGlu3-x) degradation *ex vivo*, we used brain sections of human amyloid precursor protein (hAPP)-transgenic Tg2576 mice with pronounced Aβ(pGlu3-x) plaque pathology [23,44]. After incubation with PGP-1 at 37 °C for up to 24 h, a remarkable, time-dependent reduction of Aβ(pGlu3-x) immunoreactivity was observed (**Extended Data Fig. 2a**). In contrast, Aβ(pGlu3-x) immunoreactivity was not reduced after incubation of Tg2576 brain sections with PGP-2 or with the Aβ-degrading enzymes NEP and IDE (**Extended Data Fig. 1c**), which is consistent with the data from mass spectrometric analyses shown in **Extended Data Fig. 1a**.

We next asked whether reduced Aβ(pGlu3-x) immunoreactivity after incubation with PGP-1 might be due to binding of the enzyme to its substrate without cleaving off pGlu and thus masking it for subsequent immunohistochemical labeling. Since enzymatic reactions are temperature-sensitive, we monitored Aβ(pGlu3-x) immunoreactivity after incubation of Tg2576 brain sections with PGP-1 at 0 °C, 22 °C and 37 °C for 24 h. We observed highest reductions in Aβ(pGlu3-x) immunoreactivity at 37 °C incubation but almost no reduction in Aβ(pGlu3-x) immunoreactivity after incubation with PGP-1 at 0 °C (**Extended Data Fig. 2b**). In addition, the reduction in Aβ(pGlu3-x) immunoreactivity was dependent on the amount of enzyme applied to brain sections (**Extended Data Fig. 2c**) and could be prevented by the non-competitive PGP-1 inhibitor 2-pyrrolidone (**Extended Data Fig. 2d**). Moreover, PGP-1 degraded Aβ(pGlu3-x) at early stages of plaque pathology in brain sections of 16-month-old Tg2576 mice, but also at advanced amyloid pathology with matured plaques in brain sections of 26-month-old mice (**Extended Data Fig. 2e**).

Quantification of Aβ(pGlu3-x) degradation and Aβ(4-x) formation upon PGP-1 treatment

We next quantified the degree of Aβ(pGlu3-x) degradation and the corresponding increase in the immunoreactivity of the resulting cleavage product Aβ(4-x) generated by PGP-1 activity using pairs of Tg2576 mouse brain sections incubated in the presence or absence of PGP-1 at 37 °C for 24 h (**Fig. 2a**). We demonstrate a significant reduction of Aβ(pGlu3-x) plaque area by 0.36 mm^2 (mean difference, n = 9) (**Fig. 2b**). However, because of the much higher initial Aβ(4-x) plaque load compared to Aβ(pGlu3-x) in Tg2576 brain, alteration of Aβ(4-x) plaque area did not reach statistical significance (0.05 mm^2, mean difference, n = 9) (**Fig. 2b**). Triple immunofluorescent labeling revealed reduced Aβ(pGlu3-x) immunoreactivity, whereas Aβ(4-x) and total Aβ immunoreactivities were not substantially altered upon PGP-1 treatment of Tg2576 brain sections (**Fig. 2c**). Together, these experiments demonstrate the enzymatic degradation of Aβ(pGlu3-x) to Aβ(4-x) in Aβ plaques of Tg2576 mice by PGP-1.

For the degradation of Aβ(pGlu3-x) by PGP-1 *in vivo*, a co-localization of the enzyme and its substrate around Aβ plaques is necessary. Therefore, we performed immunohistochemical labeling of endogenous PGP-1 in Tg2576 mouse brain sections to reveal a possible association with Aβ plaques. We found that Aβ plaques were frequently surrounded by neuronal/ filamentous and punctate PGP-1 immunoreactive structures (**Fig. 2d**) which were partly co-localized with Iba1-immunoreactive microglial cells (**Fig. 2e**).

Stereotactic injection: Aβ(pGlu3-x) degradation by PGP-1 *in vivo*

Finally, we wanted to reveal whether PGP-1 can reduce Aβ(pGlu3-x) plaque load in brains of experimental animals *in vivo*. Stereotactic injection of PGP-1 into the neocortex of 5xFAD mice (**Fig. 2f**) reduced the local Aβ(pGlu3-x) plaque area by 40 % compared to the saline-injected control hemisphere (**Fig. 2g**). This effect could be blocked by co-injection of PGP-1 with its inhibitor 2-pyrrolidone (**Fig. 2g**), while injection of the inhibitor alone did not affect the Aβ(pGlu3-x) plaque area (**Fig. 2g**).

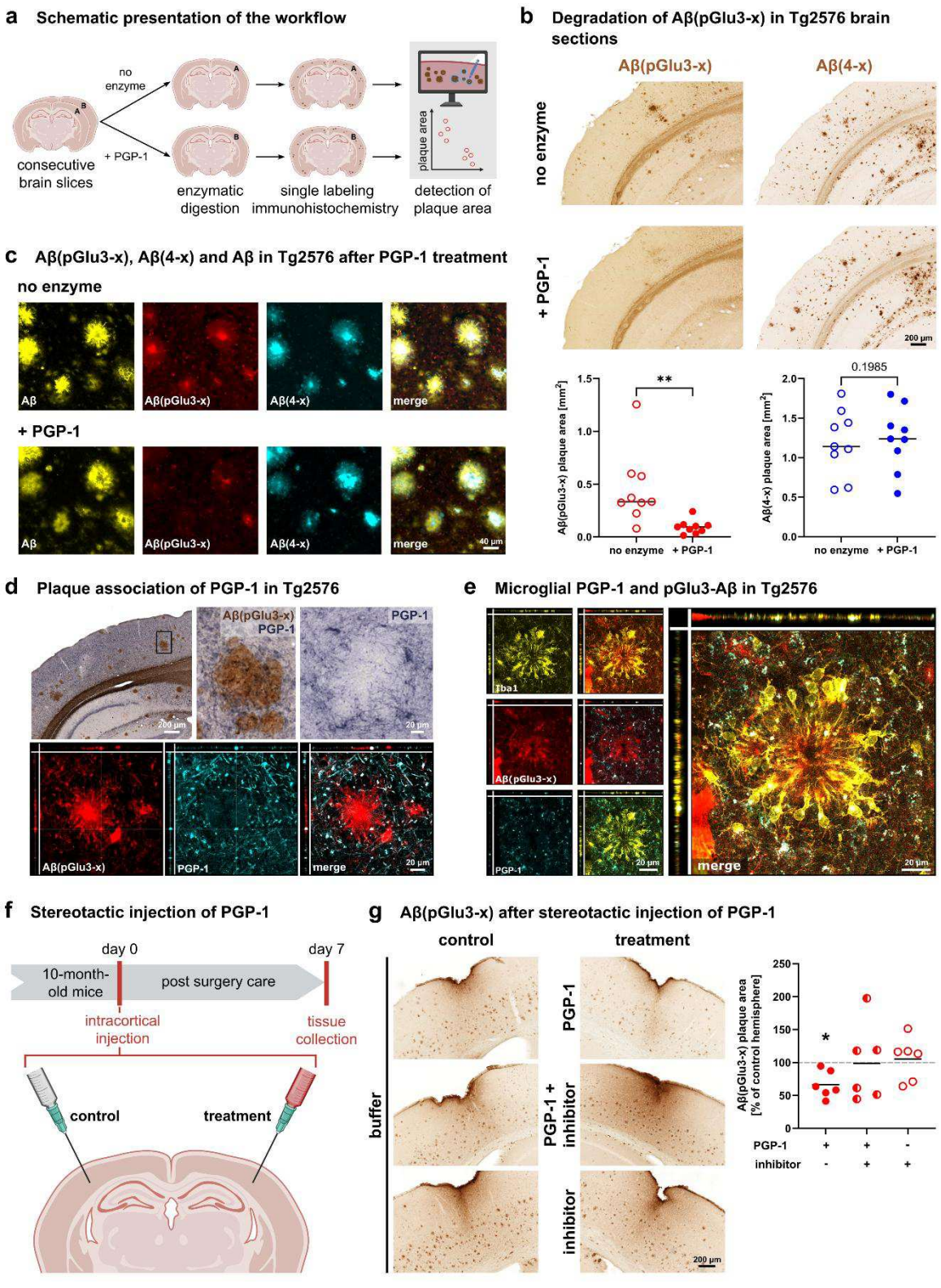


Fig. 2: Comparative quantification of Aβ(pGlu3-x) degradation and Aβ(4-x) formation after digestion of Tg2576 mouse brain sections with PGP-1 and after stereotactic injection of PGP-1 into the cortex of 5xFAD mice. a) Schematic representation of the immunohistochemical workflow. Consecutive brain sections were incubated with or without PGP-1 at 37 °C for 24 h and stained for Aβ(pGlu3-x) or Aβ(4-x) with single labeling immunohistochemistry. Plaque areas were detected using automated image analysis. Created in BioRender. Rossner, S. (2026) https://BioRender.com/vo5rbpg. **b)** Top, typical examples of Aβ(pGlu3-x) and Aβ(4-x) immunoreactivity in brain sections of an 18-month-old Tg2576 mouse. Note the much higher Aβ(4-x) immunoreactivity compared to Aβ(pGlu3-x). Bottom, quantification of Aβ(pGlu3-x) and Aβ(4-x) plaque areas of consecutive mouse brain sections incubated

with or without PGP-1 at 37 °C for 24 h. Paired two-tailed t-test, n = 9 biologically independent animals were analyzed. Medians are indicated by black line; ** $p < 0.01$. Aβ(pGlu3-x) plaque density was significantly reduced ($p = 0.0065$), whereas the initially higher Aβ(4-x) plaque load is not significantly changed ($p = 0.1985$). **c)** Examples of triple immunofluorescent labeling for the simultaneous detection of Aβ(pGlu3-x), Aβ(4-x) and pan-Aβ (MOAB-2) immunoreactivity on consecutive mouse brain sections after incubation in the absence or presence of PGP-1 at 37 °C for 24 h. **d)** In Tg2576 mouse brain, PGP-1 appeared as punctate and neuronal/ filamentous immunoreactivity enriched in the proximity of Aβ(pGlu3-x)-immunoreactive plaques and **e)** was partly co-localized to Iba1-positive microglia. **f)** Schematic representation of stereotactic injections of PGP-1 in 5xFAD mouse brain. Bregma -1.58 mm; dorsoventral -0.7 mm (from Dura), midline +/-2.75 mm. Group I received injections of PGP-1 into the left cortex, while group II received injections of PGP-1 plus inhibitor and group III the inhibitor alone (treatment). Mice of all experimental groups received injections of buffer into the right cortex at the same stereotactic coordinates (control). Schematic representation of the injection site and coronal level of the analyzed brain sections. Created in BioRender. Rossner, S. (2026) https://BioRender.com/ansau2y. **g)** Quantification of the Aβ(pGlu3-x) plaque area as a percentage of the control hemisphere in the three treatment groups. Paired two-tailed t-test, for all three treatment groups: n = 6 biologically independent animals were analyzed. Medians are indicated by black line, * $p < 0.05$. 100 % of Aβ(pGlu3-x) plaque area of control hemisphere is indicated by a dashed grey line. At the site of PGP-1 injection, a local reduction of the Aβ(pGlu3-x) plaque load by 40 % compared to the control hemisphere was quantified ($p = 0.0418$), which was not detected when the PGP-1 inhibitor 2-pyrrolidone was co-injected with PGP-1 or when the inhibitor alone was injected. Scale bars apply to all micrographs in the respective panel.

PGP-1 expression in mouse brain

There is only limited information available on the expression of *Pgpep1* mRNA and PGP-1 protein in mouse brain and peripheral organs and its brain region- and cell type-specific as well as subcellular localization. Therefore, *Pgpep1* mRNA expression was monitored in mouse brain and peripheral organs by reverse transcription quantitative PCR (RT-qPCR) and immunohistochemistry. Immunohistochemistry revealed widespread moderate neuronal PGP-1 expression in neocortex, especially in layer V, and hippocampus and very strong PGP-1 immunoreactivity in a minor neocortical and hippocampal neuronal population outside the granular and pyramidal cell layers (**Extended Data Fig. 3a**). PGP-1 immunoreactivity was also abundant in Purkinje cells of the cerebellum (**Extended Data Fig. 3b**). Triple immunofluorescent labeling identified co-expression of PGP-1 in parvalbumin-, calbindin- and somatostatin-immunoreactive neocortical interneurons (**Extended Data Fig. 3c**) and on the subcellular level revealed a co-localization with the Golgi marker syntaxin-6 in addition to its cytoplasmic localization (**Extended Data Fig. 3d**). The neuronal PGP-1 immunoreactivity did not differ between wild type and Tg2576 mice. In RT-qPCR experiments, *Pgpep1* mRNA was identified in brain tissue, with slightly lower levels found in the hindbrain than in the forebrain and midbrain (**Extended Data Fig. 3e**). Furthermore, we observed high abundance of *Pgpep1* transcripts in kidney and liver, followed by heart, spleen, stomach, intestines and duodenum (**Extended Data Fig. 3f**). Further information on RT-qPCR data can be found in **Extended Data Fig. 4** and **Suppl. Data 1**.

Human brain tissue

For translational aspects, we analyzed whether PGP-1 is also able to degrade Aβ(pGlu3-x) in plaques that matured in human AD brains for up to decades. Following the procedure established for Aβ(pGlu3-x) degradation by PGP-1 in Tg2576 mouse brain sections, we demonstrate a significant reduction of Aβ(pGlu3-x) load by 2.42 mm^2 (mean difference, n = 9) and a concomitant change of Aβ(4-x) by 4.28 mm^2 (mean difference, n = 9) (**Fig. 3a**). Triple immunofluorescent labeling revealed reduced Aβ(pGlu3-x) immunoreactivity, whereas Aβ(4-x) and total Aβ immunoreactivities were not substantially altered upon PGP-1 treatment of AD brain sections (**Fig. 3b**). To investigate the endogenous localization of the enzyme PGP-1 and its substrate Aβ(pGlu3-x), we performed immunohistochemical labeling for PGP-1 in AD brain tissue and found that Aβ plaques were frequently surrounded by neuronal and punctate PGP-1 immunoreactivity (**Fig. 3c**).

We next wanted to reveal whether PGP-1 degrades Aβ(pGlu3-x) present in advanced aggregation stages, i.e. in the FA-soluble preparation of AD brain homogenates and whether changes in the abundance of Aβ variants after PGP-1 digestion were detectable by immunoprecipitation-mass spectrometry (IP-MS) with 4G8 (**Fig. 3d**). Strikingly, in mass spectrometric analyses, peaks of the pGlu-modified Aβ peptide species (Aβ(pGlu3-40), Aβ(pGlu3-42) and Aβ(pGlu11-42)) were almost absent after PGP-1 digestion of AD brain homogenates whereas peaks for all corresponding Aβ variants after pGlu removal (Aβ(4-40), Aβ(4-42) and Aβ(12-42)) were robustly increased (**Fig. 3e**). Noteworthy, all other Aβ variants such as Aβ(1-40) and Aβ(1-42) remained unaffected by PGP-1 treatment (**Fig. 3e**). The quantification of normalized mass spectrometric peaks for the Aβ variants substantiates these effects irrespective of normalization to the sum intensity of all signals except for the spike signal (**Fig. 3f**) or to the intensity of the spike signal alone (**Extended Data Fig. 5a**). To exclude antibody-dependent effects, we also performed IP-MS using antibodies with a different selectivity to 4G8. We used a mixture of 280F2 and 12F4, capturing the C-termini of Aβ(x-40) and Aβ(x-42), respectively, and confirmed the effects seen with 4G8 (**Extended Data Fig. 5b-d**). This clearly demonstrates the efficacy and superior specificity of PGP-1 to degrade pGlu-modified Aβ peptides in human brain tissue.

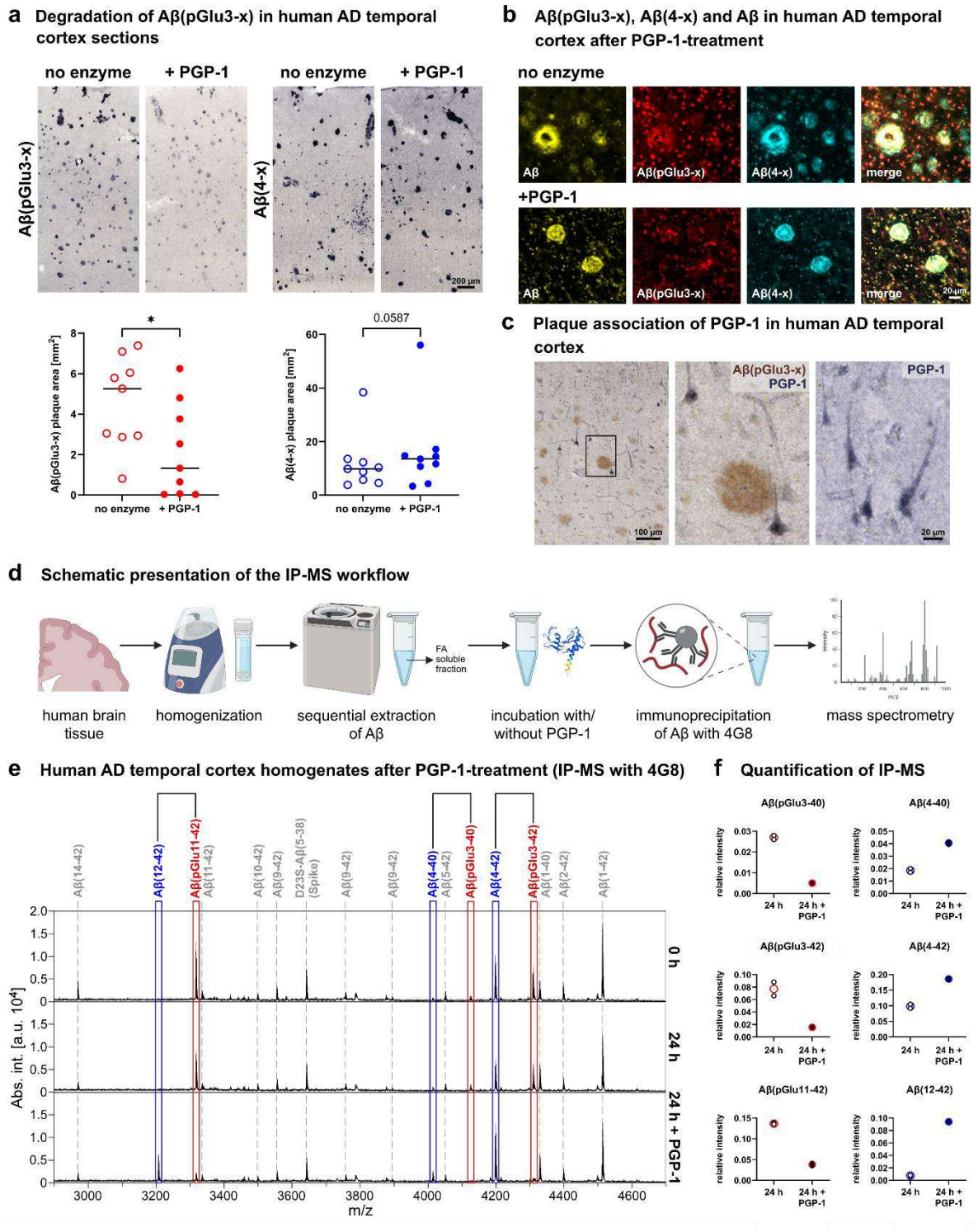


Fig. 3: Comparative quantification of Aβ(pGlu3-x) degradation and Aβ(4-x) formation after digestion of human AD brain tissue with PGP-1. a) Top, typical examples of Aβ(pGlu3-x) and Aβ(4-x) immunoreactivity in brain sections of an AD subject. Note the comparable abundance of Aβ(pGlu3-x) and Aβ(4-x) immunoreactivities prior to digestion with PGP-1 (no enzyme). Bottom, quantification of Aβ(pGlu3-x) and Aβ(4-x) plaque areas of consecutive human brain sections with or without PGP-1 digestion at 37 °C for 24 h. Paired two-tailed t-test, n = 9 biologically independent human AD patients were analyzed. Medians are indicated by black line; * $p < 0.05$. Aβ(pGlu3-x) plaque density appeared significantly reduced ($p = 0.0122$), whereas Aβ(4-x) plaque load was not significantly changed ($p = 0.0587$). **b)** Examples of triple immunofluorescent labeling for the simultaneous detection of Aβ(pGlu3-x), Aβ(4-x) and pan-Aβ (MOAB-2) immunoreactivity on brain sections after incubation in the absence or presence of PGP-1 at 37 °C for 24 h. **c)** In human AD brain, PGP-1 appeared as neuronal

and punctate immunoreactivity enriched in the proximity of Aβ(pGlu3-x)-immunoreactive plaques. **d)** Schematic representation of the IP-MS workflow. Human AD brain tissue homogenates were incubated in the absence or presence of PGP-1 at 37 °C for 24 h and analyzed by mass spectrometry after immunoprecipitation of Aβ peptides with the pan-Aβ antibody 4G8. Created in BioRender. Rossner, S. (2026) https://BioRender.com/va71u43. **e)** Mass spectra showing the changes in abundance of different Aβ peptides in human brain homogenates (pooled sample of AD1 to AD10) after incubation with PGP-1 at 37 °C for 24 h. IP-MS was performed with the pan-Aβ antibody 4G8. The substrate/ product pairs are boxed in red and blue, respectively. One representative mass spectrum out of two per condition is shown. **f)** Quantification of selected Aβ signals relative to the sum intensity of all signals in the mass range 2900-5000 m/z (except for the signal of the spike peptide D23S-Aβ(5-38)). Large red or blue dots/ circles show the mean of the two technical replicates (small black dots/ circles). Quantification demonstrates the almost complete degradation of Aβ(pGlu3-40/42) and Aβ(pGlu11-42) variants present in human brain tissue homogenates and the corresponding increase in the respective truncated Aβ variants. All other Aβ variants detected by mass spectrometry, such as Aβ1-40 and Aβ1-42, remained unaffected by PGP-1. Scale bars apply to all micrographs in the respective panel.

Comparative analyses of Aβ(pGlu3-x) and Aβ(4-x) fibril formation and toxicity

Since the degradation of Aβ(pGlu3-x) by PGP-1 results in the formation of Aβ(4-x), we considered it important to compare the aggregation characteristics and toxicities of both Aβ species in side-by-side experiments. In order to monitor fibril formation, we analyzed the respective Aβ variants in thioflavin T (ThT) aggregation assays and compared the results to the aggregation characteristics of Aβ with an intact N-terminus (**Fig. 4a**). The Aβ(pGlu3-40/42) variants displayed shorter lag phases and shorter t50 times than their Aβ(1-40/42) counterparts. The Aβ(4-42) peptides, on the other hand, showed longer lag phases and t50 times than Aβ(pGlu3-42), indicating slower aggregation characteristics (**Fig. 4a**). In addition, representative transmission electron microscopic (TEM) images revealed a shorter and thicker appearance of Aβ(pGlu3-x) fibrils compared to fibrils of Aβ with an intact N-terminus, which was not observed for the Aβ(4-x) fibrils (**Fig. 4b**).

The toxicity of monomeric and aggregated Aβ(1-40/42), Aβ(pGlu3-40/42) and Aβ(4-40/42) was assessed in differentiated mouse GT1-7 cells (**Fig. 4c**) by WST-8 assays after 24 h incubation with the respective peptides (**Fig. 4d**). In addition, continuous microscopic imaging of MitoTracker, which labels active mitochondria as an indicator of neuronal viability, was performed for 24 h (**Fig. 4e-g**). In WST-8 assays, GT1-7 cell viability was significantly lower when aggregated Aβ(1-42), Aβ(pGlu3-42) and Aβ(4-40) were added, compared to the monomeric forms of these proteins (**Fig. 4d**). No statistical differences were observed using microscopic imaging of MitoTracker on GT1-7 cells at the 24 h time point (**Fig. 4e**). Over the course of 24 h, continuous imaging of MitoTracker on GT1-7 cells showed a reduced viability of aggregated Aβ(pGlu3-40) compared to aggregated Aβ(1-40) or Aβ(4-40) (**Fig. 4f**). For both Aβ(x-40) and Aβ(x-42) species, a higher toxicity of the aggregated compared to the monomeric peptides was detected over the course of 24 h (**Fig. 4f-g**).

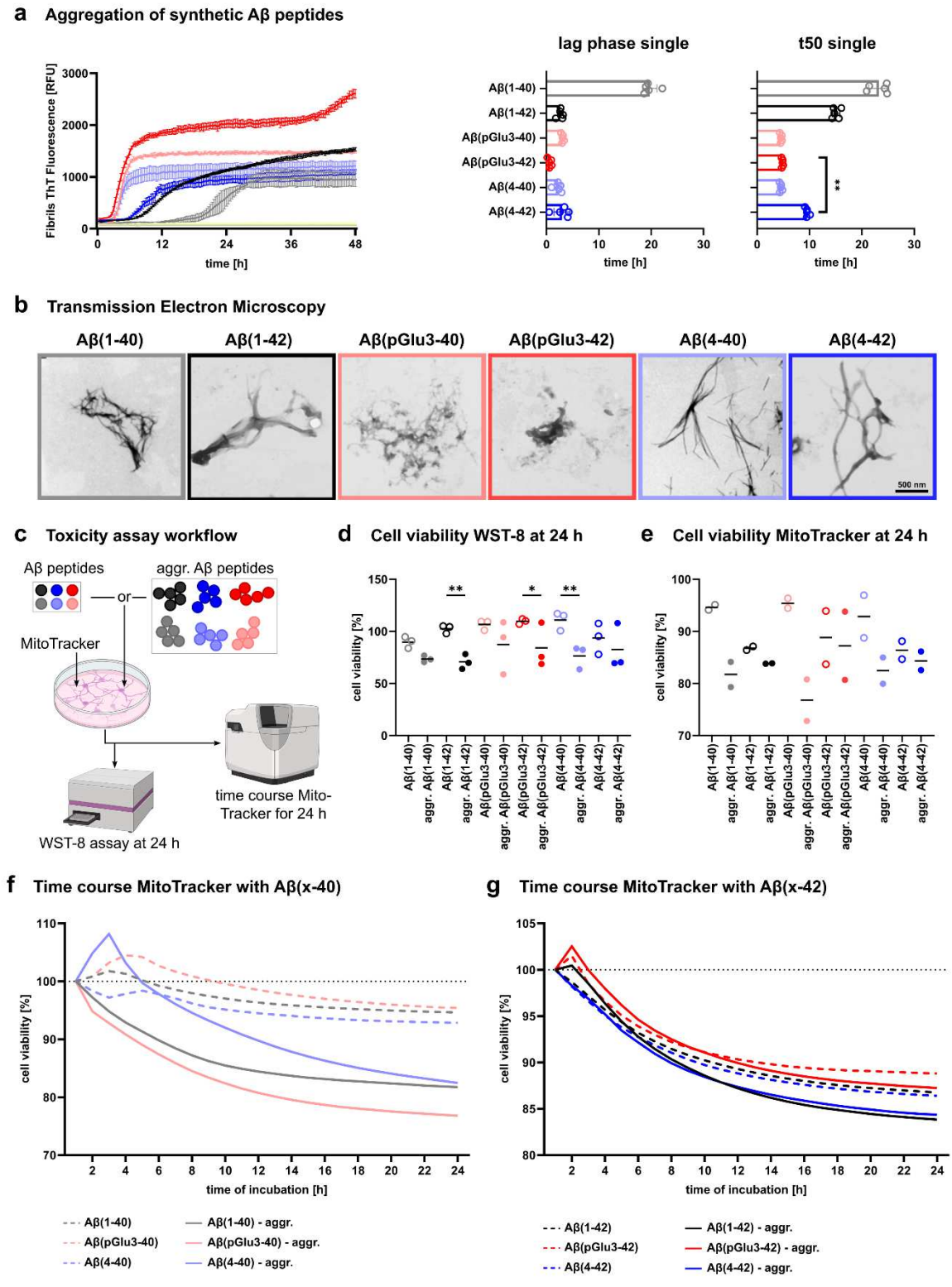


Fig. 4: Comparative analyses of synthetic Aβ peptide aggregation and toxicity. a) ThT aggregation characteristics of Aβ(1-40), Aβ(1-42), Aβ(pGlu3-40), Aβ(pGlu3-42), Aβ(4-40) and Aβ(4-42) over 48 h (left) and depiction of lag phase (middle) and t50 values (right). Note the short lag phase and short t50 values of Aβ(pGlu3-40/42) variants compared to Aβ(1-40/42). Additionally, t50 of Aβ(pGlu3-42) was significantly shorter than of Aβ(4-42) ($p = 0.0079$). For each Aβ variant, 5 technical replicates were measured; two-tailed Mann Whitney test. Data represent means ± SD. As controls, ThT alone is shown in light yellow, PBS + ThT in dark yellow. **b)** TEM images of the Aβ peptides investigated. Note the short and thick appearance of Aβ(pGlu3-x) fibrils. **c)** Schematic representation of the toxicity assay workflow. GT1-7 cells were incubated with (aggregated) Aβ peptides and MitoTracker. After 24 h, WST-8 assay

was performed. MitoTracker was used to track cell viability over 24 h. Created in BioRender. Rossner, S. (2026) https://BioRender.com/q9fcqsb. **d)** Cell viability of GT1-7 cells after adding different Aβ peptides detected with WST-8 assay after 24 h. For each Aβ variant, 3 technical replicates were measured; one-way ANOVA. Means are indicated by black line, * $p < 0.05$; ** $p < 0.01$. Note the reduced cell viability after incubation with aggregated Aβ peptides (Aβ(1-42) vs. aggr. Aβ(1-42): $p = 0.008$; Aβ(pGlu3-42) vs. aggr. Aβ(pGlu3-42): $p = 0.03$; Aβ(4-40) vs. aggr. Aβ(4-40): $p = 0.004$). **e)** Cell viability of GT1-7 cells after adding different Aβ peptides detected with MitoTracker after 24 h. For each Aβ variant, 2 technical replicates were measured. **f-g)** 24-hour time course of cell viability of GT1-7 cells performed with MitoTracker after adding (aggregated) Aβ(x-40) peptides (**f**) and (aggregated) Aβ(x-42) peptides (**g**). 100 % of cell viability is indicated by a dashed grey line. Scale bar applies to all micrographs in the respective panel.

Effect of PGP-1 on physiological substrates

Finally, we wanted to investigate whether PGP-1 might also influence physiological pGlu-modified peptides. We used brain sections of 5xFAD mice and incubated one out of two consecutive brain sections with PGP-1 at 37 °C for 24 h. Then, we performed immunohistochemical stainings for TRH and CCL2, which are both pGlu-modified under physiological conditions. Neither pGlu-TRH nor CCL2 immunoreactivity was reduced after incubation of 5xFAD brain sections with PGP-1 at 37 °C for 24 h (**Extended Data Fig. 6**).

Discussion

This is the first report on the selective enzymatic degradation of Aβ(pGlu3-x) in existing Aβ aggregates in brain. Our approach complements already available strategies on the prevention of Aβ(pGlu3-x) formation by QC inhibition and on the targeting of Aβ(pGlu3-x) with passive immunization by an alternative, antibody-independent strategy. In early Aβ sequencing experiments, Mori *et al.* used PGP to facilitate the chemical sequencing reaction and concluded that Aβ(pGlu3-x) peptides exist in AD brain [45]. However, this observation was not taken up for the therapeutic application to remove this pathogenic Aβ(pGlu3-x) variant from the brain. In the set of experiments presented here, we demonstrate that PGP-1, but not PGP-2, degrades Aβ(pGlu3-x). This is of high clinical relevance since this highly toxic Aβ variant escapes N-terminal degradation by major Aβ-degrading enzymes [17,45].

The resultant Aβ(4-x), which is generated by PGP-1 activity, is also known as a major Aβ variant in AD brain [46,47], but the mechanisms of Aβ(4-x) formation are not well understood. One study demonstrated that the oligodendrocyte-specific metalloprotease ADAMTS4 generates Aβ(4-x) by proteolytic cleavage of full-length Aβ or directly from its precursor APP [48]. Our data presented here indicate that Aβ(4-x) may also arise from Aβ(pGlu3-x) upon pGlu removal by PGP-1. Intriguingly, the resultant Aβ(4-x) has been shown to be degradable by NEP similar to Aβ with an intact N-terminus [49], suggesting that removal of the pGlu residue could facilitate Aβ degradation. This is supported by the analysis of metabolic stability of different human Aβ peptides injected into the rat hippocampus, which showed that the half-life of Aβ(4-x) was significantly shorter than of Aβ(pGlu3-x) (10 min compared to 90 min), and that full-length Aβ also had a much shorter half-life (18 min) than Aβ(pGlu3-x) [17]. Moreover, a recent study demonstrated the inhibition of IDE activity by Aβ(pGlu3-x) [50]. Since IDE is a major protease for Aβ degradation [40], its inhibition may be an additional pathological mechanism of Aβ accumulation mediated by Aβ(pGlu3-x) in AD.

In mouse brain, PGP-1 was found to be expressed by cortical and hippocampal interneurons that are immunoreactive for the calcium-binding proteins parvalbumin, calbindin and somatostatin. Although studies have shown that neurons associated with perineuronal nets, including parvalbumin-positive neurons, are spared from neurofibrillary pathology in AD [51], other studies reported vulnerability of calcium-binding protein-expressing neurons in AD [52–54]. Since these neuronal populations are known to express QC [55], compromised PGP-1 expression or activity in these neurons could thus enhance Aβ(pGlu3-x) pathology.

The co-localization of Aβ(pGlu3-x) and PGP-1 in Iba1-positive, plaque-associated microglia suggests a microglial contribution to Aβ(pGlu3-x) degradation by phagocytosis and subsequent enzymatic proteolysis. Thus, targeted manipulation of specific subsets of plaque-associated microglia might serve as a therapeutic approach. Indeed, the microglial transmembrane protein 119 (TMEM119) was shown to act as co-receptor of low density

lipoprotein receptor-related protein 1 (LRP1) to facilitate Aβ phagocytosis and to slow memory loss in 5xFAD mice [56]. The specificity of distinct, spatially defined, microglial subsets for Aβ phagocytosis was also demonstrated by the clonal expansion of non-plaque-associated microglia cells in 5xFAD mice that disturb the phagocytic capacity of their plaque-associated counterparts [57]. Thus, therapeutic induction of a focal, cell type-specific PGP-1 expression might help to reduce undesirable effects of PGP-1 on physiological pGlu-modified neuropeptides, peptide hormones and cytokines [58].

We investigated the aggregation characteristics of Aβ(pGlu3-40/42) and Aβ(4-40/42) compared to their full-length counterparts Aβ(1-40/42). Especially Aβ(pGlu3-42) showed an instant fibril formation with short lag-phase in the ThT assay, followed by Aβ(pGlu3-40) and Aβ(4-40/42) with longer lag phases. This is in line with aggregation studies performed by Schilling et al., in which pGlu-modified Aβ peptides were characterized by an about 250-fold faster initial formation of aggregates in comparison to unmodified Aβ [59]. Additionally, ThT assays comparing Aβ(1-x) and Aβ(4-x) aggregation characteristics showed a faster initial aggregation of N-terminally truncated Aβ(4-x) variants than their Aβ counterparts with intact N-termini [60,61]. Interestingly, using NMR spectroscopy to monitor the conversion of visible NMR monomers and small aggregates into larger ones, Bouter et al. showed the highest aggregation propensity for Aβ(pGlu3-42), followed by Aβ(4-42) as well as Aβ(1-42) and Aβ(4-40) with similar aggregation characteristics. The Aβ(pGlu3-40) variant was not included in this study [61]. To assess the cell viability with WST-8 assay and MitoTracker, we differentiated between freshly prepared (monomeric) and aggregated Aβ variants and found a significant higher toxicity for aggregated Aβ(pGlu3-42), Aβ(1-42) and Aβ(4-40) compared to the respective monomeric peptides. In primary wild type neuronal cultures, a higher neurotoxicity of aggregated Aβ(pGlu3-42), oligomerized for 24 h, compared to non-aggregated Aβ(pGlu3-42) was reported by Nussbaum et al. [19]. Furthermore, the treatment of primary neurons with freshly prepared Aβ peptides revealed the highest toxicities for Aβ(pGlu3-42), Aβ(4-42) and Aβ(1-42) followed by Aβ(4-40) [61]. These findings are consistent with our results, where no significant differences in cell viability of GT1-7 cells were detected when treated with the described, freshly prepared Aβ peptides. In cultured neurons and astrocytes, Aβ(pGlu3-40/42) was shown to be more toxic compared to unmodified Aβ(1-40/42) counterparts using MTT assays [16]. Interestingly, Aβ(pGlu3-40) was found to be the most toxic of the analyzed variants Aβ(pGlu3-40/42) and Aβ(1-40/42) [16], which is in line with our cell viability tests using MitoTracker. Additionally, when astrocytes were treated with modified and unmodified Aβ peptides, Aβ(1-40/42) was partially degraded whereas Aβ(pGlu3-40/42) was resistant to degradation as revealed by mass spectrometry [16].

In summary, Aβ(pGlu3-40/42) was not found to be significantly more toxic than Aβ(4-40/42) or Aβ(1-40/42) in neither WST-8 assays nor microscopic imaging using MitoTracker. Therefore, the therapeutic advantage of PGP-1 degrading Aβ(pGlu3-x) to Aβ(4-x) may be due to the higher degradability of Aβ(4-x) variants, as evidenced by their shorter half-life compared to Aβ(pGlu3-x) and Aβ(1-x), as previously described [17]. The degradation of Aβ(4-x) by NEP [49] and the *in vitro* degradation of Aβ(pGlu3-24) by PGP-1 in combination with NEP or IDE, as demonstrated in this paper, support the degradation of Aβ(4-x) *in vivo* following PGP-1 treatment. However, further experiments on the brain clearance of Aβ(4-x) species after PGP-1 treatment are needed.

The applicability of the enzymatic approach for pGlu degradation presented here is not limited to targeting Aβ(pGlu3-x) in AD, but might also be relevant for other conditions characterized by pathological pGlu protein modification such as of α-synuclein in Parkinson's disease and dementia with Lewy bodies [62]. Moreover, some types of tumor cells express high levels of pGlu-modified CD47, which creates a 'don't-eat-me signal' after binding to SIRPα expressed on myeloid cells. Inhibiting pGlu formation enhances antibody-dependent phagocytosis and cytotoxicity of tumor cells and leads to an increase in neutrophil-mediated tumor cell death [63–66]. Furthermore, the major sporozoite coat protein of malaria-causing *Plasmodium falciparum* was identified to exist in a pGlu-modified version and a monoclonal antibody against this particular protein was demonstrated to confer protection against sporozoite infection by mosquito bite in a human liver-chimeric mouse model [67]. In addition, a large proportion of snake venoms possesses an N-terminal pGlu modification promoting their stabilization against proteolytic degradation [68,69]. Therefore, in addition to the prevention of pGlu modification in several conditions by QC/isoQC inhibition, removal of existing pGlu from proteins implicated in pathological cascades is suggested as an alternative strategy with a broad spectrum of potential applications ranging from neurodegeneration to cancer, malaria and snake venom toxicity.

However, when considering therapeutic PGP-1 delivery, its effect on the de-stabilization of physiological pGlu-modified neuropeptides, peptide hormones and chemokines must be taken into account [70,71]. Interestingly, PGP-1 treatment did not affect the abundance of TRH or CCL2 immunoreactivity, which are both present in pGlu-modified form, in 5xFAD mouse brain sections. The neuropeptide pGlu-TRH was reported to be a specific substrate of PGP-2 [42] and pGlu-CCL2 might escape degradation by PGP-1 due to its N-terminal pGlu-proline bond, which was reported to be a poor PGP-1 substrate [71].

Together, we here demonstrate the capacity of the enzyme PGP-1 to degrade toxic and aggregation-prone Aβ(pGlu3-x) in brains of AD subjects and transgenic mice in a highly specific manner *ex vivo*. Furthermore, intracortical PGP-1 injection reduced the Aβ(pGlu3-x) load in a transgenic AD mouse model *in vivo*. We suggest therapeutic targeting of toxic pGlu-modified peptides, such as Aβ(pGlu3-x) in AD by a focal, cell type-specific enhancement of PGP-1 expression. Since Aβ(pGlu3-x) is involved in other neurodegenerative diseases like vascular AD or dementia with Lewy bodies [12], PGP-1 application could be also considered as a potential therapeutic approach for these conditions.

Materials and methods

Antibodies

For immunohistochemical labeling and immunoassay analyses, mainly commercial primary antibodies specific for the respective antigen were used (**Table 1**). The antibody raised against Aβ(pGlu3-x) (J8) was generated by Fraunhofer IZI-MWT (Halle, Germany) [12] and its specificity against Aβ(pGlu3-x) was previously demonstrated [72]. For the detection of Aβ(4-x), the polyclonal rabbit antibody 58-1 was used for immunohistochemical labeling [73,74]. For immunohistochemical analyses, biotinylated donkey anti-mouse, -rabbit or -goat antibodies were used as secondary antibodies (Dianova, BIOZOL Diagnostica Vertrieb GmbH, Hamburg, Germany). For immunofluorescent detection, Cy2-, Cy3- or Cy5-conjugated antibodies (Dianova, BIOZOL Diagnostica Vertrieb GmbH, Hamburg, Germany) or biotinylated secondary antibodies together with Cy7-conjugated streptavidin (AAT Bioquest, Pleasanton, CA, USA) were employed.

Mouse brain study

Animal models

APP-transgenic Tg2576 mice developed and described earlier [44] were used as a model for amyloid pathology for immunohistochemical and biochemical analyses. These mice express hAPP695 with the Swedish double mutation (K670N, M671L) as transgene under control of a hamster prion protein promoter on a mixed C57BL/6 x SJL background. Mice were housed with *ad libitum* access to water and dried, pelleted standard rodent chow (ssniff Spezialdiäten GmbH, Soest, Germany) with 12 h day/12 h night cycles. The cages contained red plastic houses and shredded paper flakes to allow nest building. At the age of six weeks, transgenicity of the animals was tested by polymerase chain reaction of ear punch-extracted DNA [44]. Female mice heterozygous for the transgene and wild type littermates were studied at ages between 15 and 28 months. All methods were carried out in accordance with the relevant guidelines and regulations (TVV16/21).

To investigate the effect of cortical PGP-1 injection, female 5xFAD mice were used. These mice carry five mutations, three in the amyloid precursor protein (APP695) gene [APP K670N/M671L (Swedish), I716V (Florida), V717I (London)] as well as two mutations in the presenilin-1 gene [PS1 M146L, L286V] [75]. The expression of the 5xFAD transgene is driven by the neuron specific Thy1 promoter. All animal experiments and procedures conformed to the Austrian guidelines for the care and use of laboratory animals (Tierversuchsgesetz 2012-TVG 2012, BGBl. I Nr. 114/2012). Animal housing, treatment, testing and euthanasia were approved by the Styrian government (GZ: ABT13-400720/2024; Amt der Steiermarkischen Landesregierung, Abteilung 13 – Umwelt und Raumordnung Austria). A total of 18 5xFAD female mice were provided by Scantox Neuro GmbH (Grambach, Austria). Mice were single

housed due to surgical procedures. Animals were housed under a constant light cycle (12 h light/dark). Dried, pelleted standard rodent chow (Altromin Spezialfutter GmbH & Co. KG, Lage, Germany) as well as water was available to the animals *ad libitum*. At an age of approximately 10 months, mice were injected bilaterally into the cortex with PGP-1 (n = 6), PGP-1 + inhibitor (n = 6) or inhibitor alone (n = 6) into the left cortex and vehicle (buffer control) into the right cortex with anterior/posterior: Bregma -1.58 mm; midline: +/-2.75 mm; dorsoventral: -1.4 mm (from Bregma), -0.7 mm (from Dura). Mice were randomly allocated to the treatment groups. An ink-test was performed prior to the first stereotactic injection to verify the correct anatomical localizations of the injection sites. PGP-1 was used at a concentration of 4.4 µg/ml. As an inhibitor, 2-pyrrolidone was used at a concentration of 100 mM [70]. Hamilton micro liter syringes at an approximate speed of 0.2 µl/min (2 µl PGP-1, inhibitor, PGP-1 + inhibitor or buffer in 10 min) with 5 min resting time were used for the injection. For inhalation anesthesia, an isoflurane vaporizer was used. Anesthesia was induced with a concentration of 4.5 - 5 % isoflurane and maintained during surgery with a concentration of 1.5 - 2 % isoflurane. For pain management, Buprenorphine 0.1 mg/kg was administered *intraperitoneal* at least 15 min before pain was inflicted using an application volume of 10 µl per g mouse body weight. Vital functions were checked regularly during the surgery. After injection wounds were closed with a surgical suture and if necessary, tissue adhesive was applied. After the surgery, animals were observed intensively for seven days in order to check the tolerability of the injection (three times daily the first three days and afterwards once per day for the remaining days). One week after surgery, animals were euthanized and tissue was collected.

Mouse tissue preparation

Tg2576 mice were sacrificed by CO_2 inhalation and 5xFAD mice were terminally anesthetized by injection of Pentobarbital (600 mg/kg, dosing 10 µl/g body weight) by Scantox Neuro GmbH. Mice were perfused transcardially with 0.9 % saline, followed by perfusion with 4 % paraformaldehyde in phosphate buffer (0.1 M; pH 7.4). The brains were removed from the skull and post-fixed by immersion in the same fixative for 24 h at 4 °C. After cryoprotection in 30 % sucrose in 0.1 M phosphate buffer for three days, 30 µm thick coronal sections were cut on a sliding microtome and collected in phosphate buffer supplemented with 0.0025 % sodium azide for storage at 4 °C.

PGP-1 assay on mouse brain sections

In order to test the ability of PGP-1 to degrade Aβ(pGlu3-x) on fixed coronal brain sections, one brain section out of two consecutive brain sections was incubated with PGP-1 (**Table 3**; R&D Systems, Bio-Techne Corporation, Minneapolis, MN, USA) at a concentration of 4.4 µg/ml in 0.1 M potassium phosphate buffer containing 1 mM ethylenediaminetetraacetic

acid (EDTA) and 0.5 mM dithiothreitol (pH 7.4), further referred to as PGP-1 buffer, at 37 °C for 24 h. Since the two consecutive brain sections were identical in overall size, they were only supposed to differ in total plaque area depending on whether they had received PGP-1 treatment. Measurement of the respective total plaque areas was later used as a readout for the PGP-1 reaction (see *Automated image analysis and statistics*). Varying PGP-1 concentrations in a range between from 0.2 µg/ml to 4.4 µg/ml, temperatures between 0 °C and 37 °C as well as incubation times between 0 h to 24 h were used for the initial characterization of the PGP-1 reaction. As an inhibitor for PGP-1, 2-pyrrolidone was used at concentrations of 1 µM, 100 µM and 100 mM as indicated [70].

PGP-2, NEP and IDE assay on mouse brain sections

In order to test the ability of PGP-2, NEP and IDE to degrade Aβ(pGlu3-x) on fixed coronal brain sections, one brain section out of two consecutive brain sections was incubated with PGP-2, NEP or IDE (**Table 3**; R&D Systems, Bio-Techne Corporation, Minneapolis, MN, USA). Enzyme concentrations and incubation times, which varied between 24 h and 96 h, were adjusted to achieve a similar level of specific activity to that of PGP-1 (**Table 3**) in the PGP-1 assay. For PGP-2 incubation, 20 mM potassium phosphate buffer (pH 7.5) was used. The incubation with NEP and IDE was carried out in 100 mM Tris-HCl buffer (100 mM Tris, 50 mM sodium chloride, 10 µM zinc chloride, pH 7.5). The two consecutive brain sections were identical in overall size and the plaque areas were later used as a readout for the enzyme reaction.

Mouse single and double labeling immunohistochemistry

Single labeling immunohistochemistry on free-floating coronal brain sections was carried out according to Bluhm et al. [76] In short, brain sections were initially washed in 0.1 M phosphate buffer (pH 7.4) for 5 min. All other washing steps between incubation steps were carried out in 0.1 M Tris-buffered saline (TBS; pH 7.4) for 5 min each, unless stated otherwise, and are not mentioned further. First, endogenous peroxidases were inactivated by treating brain sections with 60 % methanol containing 1 % H_2O_2 for 60 min. After masking unspecific binding sites with blocking solution (5 % normal donkey serum in TBS containing 0.3 % Triton X-100) for 60 min, sections were incubated with the primary antibodies at 4 °C for 40 h (**Table 1**). When primary antibodies of mouse origin were used, the blocking solution contained 2 % normal donkey serum and 3 % donkey Fab fragments directed against mouse immunoglobulins. After incubating the brain sections with biotinylated donkey anti-mouse, anti-rabbit or anti-goat secondary antibodies (1:1,000; Dianova, BIOZOL Diagnostica Vertrieb GmbH, Hamburg, Germany), respectively, in TBS containing 2 % bovine serum albumin (BSA) for 60 min, sections were treated with ExtrAvidin peroxidase (1:2,000; Sigma-Aldrich, Merck KGaA,

Darmstadt, Germany) in TBS with 2% BSA. Brain sections were then pre-incubated in Tris buffer (0.05 M, pH 7.6 for 3,3'-diaminobenzidine (DAB) staining and 0.05 M, pH 8,0 for DAB staining with ammonium nickel(II) sulfate (DAB-Ni)) for 5 min. Finally, visualization of peroxidase binding was performed by incubation with 4 mg DAB and 2.5 µl H_2O_2 per 5 ml Tris buffer (0.05 M, pH 7.6) yielding brown epitope staining or with 1 mg DAB, 20 mg ammonium nickel(II)sulfate and 2.5 µl H_2O_2 per 5 ml Tris-buffer (0.05 M; pH 8.0) yielding black epitope staining. Sections were mounted onto glass slides and cover slipped. Omitting the primary antibody (negative control) did not generate immunohistochemical labeling (not shown).
Combined immunohistochemical labeling of Aβ(pGlu3-x) (brown, DAB) and PGP-1 (black, DAB-Ni) was performed sequentially. First, PGP-1 was labeled with DAB-Ni to produce a black precipitate. Then, Aβ(pGlu3-x) was labeled with DAB, yielding a brown precipitate.

Mouse triple immunofluorescent labeling

In order to reveal the possible co-localization of PGP-1 with Aβ(pGlu3-x), Iba1, parvalbumin, calbindin, somatostatin, syntaxin 6 and calreticulin, respectively, in the mouse brain, cocktails of three primary antibodies from different species were applied as specified in **Table 1**.
Triple immunofluorescent labeling on free-floating coronal brain sections was carried out according to Bluhm et al. [76] In short, brain sections were initially washed in 0.1 M phosphate buffer (pH 7.4) for 5 min. All other washing steps between incubation steps were carried out in 0.1 M Tris-buffered saline (TBS; pH 7.4) for 5 min each and are not mentioned further. First, brain sections were incubated in 60 % methanol for 60 min followed by masking unspecific binding sites with blocking solution (see *Mouse single and double labeling immunohistochemistry*). Brain sections were incubated with primary antibody cocktails at 4 °C for 40 h (**Table 1**). Subsequently, sections were incubated with cocktails of Cy2-, Cy3- or Cy5-conjugated donkey anti-mouse, -goat, -guinea pig, -rabbit or -chicken antisera (1:400 each; Dianova, BIOZOL Diagnostica Vertrieb GmbH, Hamburg, Germany) in TBS containing 2 % BSA for 60 min. Next, sections were mounted onto glass slides before being cover slipped. In control experiments, switching the fluorescent labels of the secondary antibodies generated similar results (not shown). In addition, omitting primary antibodies (negative control) did not generate immunohistochemical labeling (not shown).
Triple labeling of the antigens Aβ(pGlu3-x), Aβ(4-x) and Aβ showed some deviations from the normal protocol. First, unspecific binding sites were masked with blocking solution containing 2 % normal goat serum and 3 % goat Fab fragments directed against mouse immunoglobulins. Second, the incubation with primary antibody cocktails at 4 °C for 40 h was followed by incubation with cocktails of Cy3-conjugated goat anti-mouse antisera specific for immunoglobulin G (IgG) subtype IgG2a, Cy5-conjugated goat anti-rabbit and biotinylated goat anti-mouse antisera specific for IgG subtype IgG2b (1:500 each; Dianova, BIOZOL

Diagnostica Vertrieb GmbH, Hamburg, Germany) in TBS containing 2 % BSA for 60 min. Third, brain sections were incubated in Cy7-conjugated streptavidin (1:200, AAT Bioquest, Pleasanton, CA, USA) in TBS containing 2 % BSA for 60 min.

Human brain study

Human brain tissue

The human brain tissue (AD1 to AD10, **Table 2**) was provided by the Arizona Study of Aging and Neurodegenerative Disorders (AZSAND) and Brain and Body Donation Program of Banner Sun Health Research Institute in Sun City, Arizona. Autopsy was performed as approved by institutional review boards overseeing AZSAND's Brain and Body Donation Program [77]. The required consent was obtained for all cases. The diagnosis of AD cases was based on the presence of neurofibrillary tangles and amyloid and neuritic plaques in subcortical and neocortical areas and met "intermediate" or "high" levels of AD Neuropathological Change according to the criteria of the National Institute on Aging - Alzheimer's Association (NIA-AA). Brain sections of the posterior superior temporal gyrus (Brodmann area 22) from ten AD cases were used for immunohistochemical and biochemical evaluations. Biochemical analyses were performed in unfixed brain tissue from the same location (Brodmann area 22) of the other brain hemisphere of the same cases. For detailed characterization of the cases, see **Table 2**.

Human brain tissue for immunohistochemical analyses was supplemented with tissue (AD11 to AD17, **Table 2**) provided by the Paul Flechsig Institute - Center for Neuropathology and Brain Research at the Leipzig University Medical Faculty, the Department of Neuropathology Leipzig, following ethical guidelines and with valid ethical vote. The entire procedure of acquisition of the patient's personal data, the protocols and the informed written consent forms of all participants or the relatives of the deceased patients as well as performing the autopsy and handling the autopsy material have been approved by the responsible authorities (approval by the Ethics Committee of the University of Leipzig; approval #205/17-ek). The study was conducted in accordance with the principles expressed in the Declaration of Helsinki. Neuropathological assessment revealed no signs of significant neurological diseases. The diagnosis and staging of AD cases used in this study were based on the presence of neurofibrillary tangles [78] and neuritic plaques in subcortical and neocortical areas as outlined by the Consortium to establish a registry for AD (CERAD) [79] and met the criteria of the National Institute on Aging (NIA) on the likelihood of dementia [80]. Temporal cortex (Brodmann area 22) from 7 AD cases was used. For detailed characterization of the cases see **Table 2**.

Human brain tissue preparation

Tissue blocks of the human temporal cortex (AD1 - AD10) were prepared in coronal brain slices of 1.0 cm thickness, rinsed in phosphate buffer and immersed in 10 % neutral buffered

formalin at 4 °C for 48 h. Following fixation, slices were sequentially transferred to cryoprotectant solutions containing 2 % dimethyl sulfoxide and 10 % glycerol for 48 h, followed by 2 % dimethyl sulfoxide and 20 % glycerol for an additional 48 h. Then, 40 - 80 µm thick sections were cut on a microtome and collected in in cryoprotectant solution.
Tissue blocks of the human temporal cortex (AD11 - AD17) were prepared in the frontal plane, fixed in 4 % paraformaldehyde and cryoprotected in 30 % sucrose in 0.1 M phosphate buffer (pH 7.4) before sectioning. Then, 30 µm thick sections were cut on a freezing microtome and collected in 0.1 M phosphate buffer containing 0.1 % sodium azide.

PGP-1 assay on human brain sections

In order to test the ability of PGP-1 to degrade Aβ(pGlu3-x) on *post mortem* human brain tissue, one brain section out of two consecutive brain sections was incubated with PGP-1 (**Table 3**; R&D Systems, Bio-Techne Corporation, Minneapolis, MN, USA) at a concentration of 4.4 µg/ml in PGP-1 buffer at 37 °C for 24 h. Since the two consecutive brain sections were identical in overall size, they were only supposed to differ in total plaque area depending on whether they had received PGP-1 treatment. The plaque areas were later used as a readout for the PGP-1 reaction (see *Automated image analysis and statistics*).

Human single and double labeling immunohistochemistry

Single labeling immunohistochemistry on free-floating human brain sections was carried out according to Schrempel et al. [12] Free-floating human brain sections were washed in PBS containing 0.02 % Tween 20 (PBS-T) and treated with 1 % H_2O_2 in 60 % methanol for 60 min. Unspecific staining was blocked by incubating brain sections in blocking solution (PBS-T with 2 % (w/v) BSA, 0.3 % (w/v) milk powder, 0.5 % (v/v) normal donkey serum) for 60 min before incubating brain sections with primary antibodies in blocking solution at 4 °C for 42 h (for antibody concentrations, see **Table 1**). Brain sections were incubated in a 1:2 mixture of blocking solution and PBS-T containing the biotinylated donkey anti-mouse or anti-rabbit, respectively, secondary antibody (1:1,000 Dianova, BIOZOL Diagnostica Vertrieb GmbH, Hamburg, Germany) for 60 min followed by incubation with ExtrAvidin-conjugated peroxidase (1:2,000; Sigma-Aldrich, Merck KGaA, Darmstadt, Germany) in PBS-T for 60 min. Bound peroxidase was visualized in a solution containing 2 mg DAB, 20 mg ammonium nickel(II) sulfate and 2.5 µl H_2O_2 per 5 ml Tris-buffer (0.05 M, pH 8.0) yielding black epitope staining. Brain sections were mounted onto glass slides before being cover slipped. Omitting the primary antibody (negative control) did not generate immunohistochemical labeling (not shown).
Combined immunohistochemical labeling of Aβ(pGlu3-x) (brown, DAB) and PGP-1 (black, DAB-Ni) was performed sequentially. First, PGP-1 was labeled with DAB-Ni to produce a black precipitate. Then, Aβ(pGlu3-x) was labeled with DAB, yielding a brown precipitate.

Human triple immunofluorescent labeling

For triple immunofluorescent labeling, free-floating human brain sections were washed in PBS containing 0.02 % Tween 20 (PBS-T) and treated with 60 % methanol for 60 min. Unspecific staining was blocked by incubating brain sections in blocking solution (PBS-T with 2 % (w/v) BSA, 0.3 % (w/v) milk powder, 0.5 % (v/v) normal donkey serum) for 60 min before incubating brain sections with primary antibody cocktails in blocking solution at 4 °C for 42 h (for antibody concentrations, see **Table 1**). Brain sections were incubated in a 1:2 mixture of blocking solution and PBS-T containing the cocktails of Cy3-conjugated goat anti-mouse antisera specific for IgG2a, Cy5-conjugated goat anti-rabbit and biotinylated goat anti-mouse antisera specific for IgG2b (1:800 each; Dianova, BIOZOL Diagnostica Vertrieb GmbH, Hamburg, Germany) for 60 min followed by treatment with Cy7-conjugated streptavidin (1:100, AAT Bioquest, Pleasanton, CA, USA) in a 1:2 mixture of blocking solution and PBS-T for 60 min. Next, sections were mounted onto glass slides before being cover slipped. In control experiments, switching the fluorescent labels of the secondary antibodies generated similar results (not shown). In addition, omitting the primary antibody (negative control) did not generate immunohistochemical labeling (not shown).

Microscopy

Light microscopy

Immunohistochemically stained and immunofluorescent mouse and human brain sections were digitized with an AxioScan.Z1 slide scanner connected with a LED light source and a Hitachi HV-F202SCL camera (Carl Zeiss AG, Oberkochen, Germany). Using a 20x objective lens with 0.8 numerical aperture (Carl Zeiss AG, Oberkochen, Germany), images were taken and digitized with the ZEN 3.7 software (Carl Zeiss AG, Oberkochen, Germany). Images were processed using the Zeiss ZEN 3.9 imaging tool (Carl Zeiss AG, Oberkochen, Germany) and Adobe Photoshop CS2 (Adobe Systems, San José, CA, USA). Care was taken to apply the same brightness, sharpness, color saturation and contrast adjustments in the processing of the various pictures.

Analyses of fluorescence signals

The confocal laser scanning microscope LSM 880 AiryScan (Carl Zeiss Microscopy GmbH, Jena, Germany) was used for imaging of immunohistochemically stained samples. Confocal laser scanning microscopy was performed to reveal the spatial relationship of PGP-1 with Aβ(pGlu3-x), Iba1, parvalbumin, calbindin, calreticulin, somatostatin and syntaxin-6. The fluorescence was excited with an argon laser (488 nm, Cy2) and two helium-neon-lasers (563 nm, Cy3; 633 nm, Cy5). The emitted light was collected using three band-pass filters:

505 - 530 nm for Cy2, 565 - 615 nm for Cy3 and 650 - 710 nm for Cy5. Images of areas of interest were taken using a 20x objective with 0.8 numerical aperture or with a 63x immersion C-Apochromat with 1.2 numerical aperture (Carl Zeiss Microscopy GmbH, Jena, Germany).
Brain sections stained with Cy7-labeled immunoreagents were scanned with an AxioScan.Z1 microscope (Carl Zeiss Microscopy GmbH, Jena, Germany) equipped with a Colibri7 light source. Images of brain sections were taken by the Axiocam 506 and a Plan-Apochromat objective (20x/0.8 NA; Carl Zeiss Microscopy GmbH, Jena, Germany) with an exposure time of 20 ms for Cy3, 20 ms for Cy5 and 20 ms for Cy7. Images were digitized using the ZEN 3.7 software (Carl Zeiss Microscopy GmbH, München, Germany).
Zeiss ZEN 3.9 imaging tool (Carl Zeiss Microscopy GmbH, München, Germany) and Adobe Photoshop CS2 (Adobe Systems, CA, USA) were used to process the images obtained with the AxioScan.Z1 slide scanner and by confocal laser scanning microscopy. Care was taken to apply the same brightness, sharpness, color saturation and contrast adjustments in the various pictures.

Automated image analysis

To quantify the Aβ(pGlu3-x) and Aβ(4-x) stained plaque area of immunohistochemically labeled brain sections, Zeiss arivis Cloud (Carl Zeiss Microscopy GmbH, Jena, Germany) and Zeiss ZEN 3.8 Intellesis software (Carl Zeiss Microscopy GmbH, München, Germany) were used for automated image analysis. A separate training for immunohistochemically stained mouse brain tissue and human brain tissue was conducted using Zeiss arivis Cloud. After several iterating training cycles to enhance the capability of the machine learning algorithm to detect DAB or DAB-Ni-stained plaques, whole mouse or human brain sections were analyzed by the trained algorithm in a batch analysis using Zeiss ZEN 3.8 software. In case of PGP-1- and/or inhibitor-injected 5xFAD mice, immunohistochemically labeled mouse brain sections at the injection site were used. Regions of interest measuring 4.5 mm^2 around the treatment or control injection site were used for batch analysis. In general, obviously false positive detection of unspecific staining was manually removed upon visual inspection. For statistical analysis, the total Aβ(pGlu3-x) or Aβ(4-x) plaque area of each immunohistochemically stained mouse or human brain section or region of interest was calculated. Paired two-tailed t-tests were conducted to compare the plaque areas of untreated with PGP-1-treated brain sections using GraphPad PRISM 10 (San Diego, CA, USA). Differences between groups were considered statistically significant for p values < 0.05.

Power analysis

To compare Aβ(pGlu3-x) or Aβ(4-x) plaque areas of mouse and human brain sections with or without PGP-1 digestion, an *a priori* power analysis with G*Power 3.1.9 [81] was performed with

effect size d = 0.9, α error = 0.1 and power = 0.8. The analysis indicated that 16 samples per group would be required to detect the expected effect size. Input parameters for G*Power required to calculate the sample size were based on prior experience with comparable experiments. Due to limited sample availability, the study was conducted with n = 9 samples per group. Although this sample size was below that suggested by the *a priori* power analysis, statistically significant differences were observed, suggesting that the actual effect size was larger than anticipated.

For the stereotactic injection of PGP-1 and/or the inhibitor into the cortex of 5xFAD mice, an *a priori* power analysis with G*Power 3.1.9 [81] was performed with effect size d = 0.9, α error = 0.1 and power = 0.6. The analysis indicated that 10 samples per group would be required to detect the expected effect size. Due to the 3R's (Replacement, Reduction and Refinement), only 6 mice per group were used. This reduced number was sufficient to reach a significant difference.

Mass spectrometry with synthetic peptides

The Aβ(pGlu3-24) peptide (**Table 4**) was purchased from the Core Unit Peptide, University of Leipzig, dissolved in 0.1 M NaOH and neutralized with 0.1 M HCl. In order to test the capacity of enzymes to cleave Aβ(pGlu3-x), 2 µl of PGP-1 (PGP-2, NEP or IDE; **Table 3**) were diluted in PGP-1 buffer (or 20 mM potassium phosphate buffer or 100 mM Tris-HCl buffer, respectively; see *PGP-2, NEP and IDE assay on mouse brain sections*) containing 100 µM Aβ(pGlu3-24). Combined incubations of Aβ(pGlu3-24) with PGP-1 + NEP or PGP-1 + IDE were performed in PGP-1 buffer. After incubation at 37 °C for 0 min to 24 h, the enzymatic reactions were stopped by heating samples in a Thermocycler (100 °C) for 5 min and centrifugation at 13,000 rpm at room temperature for 20 min. Samples were stored at -70 °C until further usage.

For mass spectrometric analyses, 20 µl of each sample was acidified with 5 µl of H_2O/TFA (990/10; v/v) and subsequently purified using C_{18} stage-tips (5 layers). Elution was carried out with 10 µl of ACN/H_2O/TFA (750/247.5/2.5; v/v/v). The eluate was co-crystallized with 2,5-dihydroxybenzoic acid (DHB) on a MALDI ground steel target. Mass spectra were acquired on a MALDI-TOF/TOF mass spectrometer (Autoflex Speed, Bruker Daltonics, Bremen, Germany) with positive polarity in reflector mode. Spectra were recorded using flexControl (version 3.4, Bruker Daltonics, Bremen, Germany) by accumulation of at least 10,000 shots (per sample spot). Spectra processing was carried out with flexAnalysis (version 3.4, Bruker Daltonics, Bremen, Germany) by applying baseline subtraction with TopHat algorithm, smoothing with Savitzky-Golay algorithm and peak detection with SNAP algorithm. The MALDI-TOF/TOF mass spectrometer was calibrated using the mass signals of a set of standard peptides with known masses (Cat. No. 8222570, Peptide Calibration Standard II, Bruker Daltonics, Bremen,

Germany). Spectra employed for calibration were acquired with the same laser energy as used for sample analysis. Cleavage products were analyzed using the FindPept tool by Expasy [82]. Evaluation of the spectra was done using mMass version 5.5.0.

Quantifications in human brain homogenates after PGP-1 treatment

Human brain tissue preparation

Tissue blocks of human temporal cortex were prepared in the frontal plane according to the atlas of the human brain and stored at -70°C until usage. The mass spectrometric analysis of human brain homogenate after PGP-1 incubation was performed with a pooled sample of brain homogenates of AD1 to AD10 (n = 10). Brain homogenates of AD1 to AD10 were prepared according to Gnoth et al. [83] and Schrempel et al. [12] In short, a sample of about 500 mg human temporal cortex was homogenized in TBS buffer (20 mM Tris/HCl, 150 mM NaCl, 5 mM KCl, pH 7.5) supplemented with Protease Inhibitor Cocktail Tablets (Roche Diagnostics GmbH, Mannheim, Germany) and 1 mM 4-(2-Aminoethyl)-benzolsulfonylfluoride hydrochloride at a concentration of 200 mg/ml by using a Precellys homogenizer (Bertin Technologies S.A.S, Montigny-le-Bretonneux, France), followed by sonication for 10 s. After centrifugation of the homogenate at 100,000xg for 1 h, supernatant (TBS fraction) was obtained. The resulting pellet was dissolved to 250 mg/ml in 5 M guanidinium chloride (GdmCl), followed by an incubation step in an overhead shaker at room temperature for 3 h and a subsequent centrifugation step at 100,000xg for 1 h. Again, supernatant (GdmCl fraction) was collected and the pellet was resuspended in 500 µl 70 % formic acid (FA), followed by sonication for 20 s and neutralization by 2.9 ml 3.5 M Tris (FA fraction). Samples AD1 to AD10 were pooled for mass spectrometric analyses.

PGP-1 assay

To demonstrate the ability of PGP-1 to degrade Aβ(pGlu3-x) in advanced aggregation stages, human brain homogenates were used. PGP-1 assay was performed on the pooled sample of AD1 to AD10 (n = 10) FA fractions. For the immunoprecipitation-mass spectrometry, the pooled sample of AD1 to AD10 FA fractions (177 mg/ml) was used. A volume of 50 µl of the sample was incubated with 148 µl PGP-1 buffer and 2 µl of PGP-1 (0.44 mg/ml) or, in case of controls without PGP-1, with 150 µl of PGP-1 buffer at 37 °C for 0 h and 24 h, respectively. The enzymatic reaction was stopped by heating samples in a Thermocycler (100 °C) for 5 min and centrifugation at 13,000 rpm at room temperature for 20 min. Samples of pooled AD1 to AD10 were stored at -70 °C until further usage.

Immunoprecipitation-mass spectrometry with brain homogenates

The monoclonal antibodies 4G8 (Cat. No. 800702, RRID:AB_2564634; BioLegend, Inc., San Diego, CA, USA), 12F4 (Cat. No. 805501, RRID:AB_2564683; BioLegend, Inc., San Diego, CA, USA) and 280F2 (Cat. No. 218221, RRID:AB_2619921; Synaptic Systems, Göttingen, Germany) were covalently coupled to Dynabeads M-270 Epoxy (Invitrogen, Waltham, MA, USA) as described previously [84].

For immunoprecipitation, 50 µl of the FA fractions from the AD pool AD1 to AD10 used in the PGP-1 assay (with and without PGP-1 treatment, see *PGP-1 assay*) was diluted with 200 µl of 1xPBS and mixed with an equal volume of 100 mM Tris-HCl, pH 7.4 containing 0.2 % (w/v) nonyl-β-d-thiomaltoside (NTM), 0.2 % (w/v) n-dodecyl-β-d-maltoside (DDM) and either 15 µl 4G8 or 10 µl 12F4 + 10 µl 280F2 functionalized Dynabeads M-270 Epoxy carrying the respective antibodies. The samples were incubated overnight at 4 °C with constant mixing and the beads were washed 5x with 0.5 ml of 50 mM Tris-HCl, pH 7.4, 150 mM NaCl containing 0.1 % (w/v) NTM and 0.1 % (w/v) DDM, followed by a resuspension in 0.5 ml 50 mM ammonium acetate (pH ~7.0). For mass spectrometric analysis, essentially performed as described [84,85], the beads were immobilized on a magnet, the supernatant was removed, and the beads were washed 1x with 0.5 ml of 50 mM ammonium acetate and 1x with 0.5 ml H_2O. Bound Aβ peptides were eluted in 2.5 µl of 70 % acetonitrile containing 5 mM HCl. For quantification purposes, the eluent additionally contained a 50 nM final concentration of the synthetic Aβ5-38(D23S) peptide featuring an Asp to Ser amino acid substitution at position 23 to be used as a standard for spectra normalization [84]. For MALDI-TOF-MS, the eluates (0.5 µl) were spotted onto a pre-structured MALDI sample support (MTP AnchorChip 384 BC; Cat. No. 8280790, Bruker, Bremen, Germany), followed by the addition of 0.5 µl matrix solution consisting of 5 mg/ml α-cyano-4-hydroxycinnamic acid (CHCA) in 50 % acetonitrile/0.05 % trifluoroacetic acid (TFA). A 1:1 mixture of Peptide Calibration Standard II (Cat. No. 8222570, Bruker, Bremen, Germany) and PepMix2 (Cat. No. C102, LaserBio Labs, Valbonne, France) was used as calibrant. The samples were dried in a vacuum desiccator and a total of 5000 mass spectra per spot were recorded using an ultrafleXtreme MALDI-TOF/TOF mass spectrometer. The instrument was operated in reflector mode under the software flexControl 3.4 (Bruker, Bremen, Germany) and peak detection was performed with the SNAP2 algorithm implemented in the software flexAnalysis 3.4 (Bruker, Bremen, Germany). Detected peaks were quantified via their signal height and normalized either to the signal height of the spike peptide Aβ5-38(D23S) or to the sum intensity of all signals in the mass range 2900-5000 m/z (excluding the spike signal). Visualization and statistical analysis of the data was performed in GraphPad PRISM (version 10, San Diego, CA, USA).

Thioflavin T fibril formation assays

Aβ aggregation studies were based on [86]. Lyophilized Aβ peptides were dissolved in 1,1,1,3,3,3-hexafluoro-2-propanol (HFIP) to obtain homogeneous preparations without seeds. For peptide preparation, the HFIP was evaporated and immediately prior to analysis, peptide pellets were dissolved in 20 µl 0.1 M NaOH, 20 µl 0.1 M HCl and 960 µl PBS, pH 7.1. All steps were carried out on ice. Peptide concentration was adjusted to 12,5 µM. To monitor the fibril formation of Aβ variants, monomeric Aβ peptide was co-incubated with 40 µM thioflavin T (ThT) in 96-well microtiter plates (PS, half area, black µClear; Greiner Bio-One, Kremsmünster, Austria). Measurements were carried out by 5-fold determination. The plate was sealed with adhesive film and incubated at 37 °C for 48 h. Before each measurement, the plate was shaken at 600 rpm for 5 min. ThT fluorescence intensity was measured using a FLUOstar Omega (BMG Labtech, Ortenberg, Germany) plate reader (excitation 440 nm, emission 490 nm). Kinetic parameters of the ThT curves of the fibril-forming Aβ variants were calculated using logistic sigmoid functions in GraphPad PRISM 10 (San Diego, CA, USA). Mann-Whitney test was performed to investigate differences in lag phase and t50. Differences between groups were considered statistically significant for p values < 0.05.

Transmission electron microscopy

Transmission electron microscopy (TEM) of Aβ aggregates was based on [87]. In short, aggregated peptides from the ThT assay were diluted 1:100 and incubated on an EM Veco Cu Single Slot TEM Grid L2x1mm (Science Service, Munich, Germany) at room temperature for 30 min and washed three times with distilled water. After drying grids for 30 min, contrasting of fibrils was obtained with 2 % (v/v) uranyl acetate (SERVA Electrophoresis GmbH, Heidelberg, Germany) for 5 min followed by three washing steps with distilled water. Fibrils were imaged with a LEO EM 912 Omega TEM (Carl Zeiss AG) at 80 kV and digital micrographs were obtained with a dual-speed 2 K-on-axis CCD camera-based YAG scintillator and the software ImageSP (version 1.2.13.17, TRS-Tröndle, Moorenweis, Germany).

RT-qPCR in mouse tissue

2.11.1 Tissue preparation

Tg2576 mice were housed as described earlier. Female mice heterozygous for the transgene (4 months n = 1; 20 months n = 1) and female wild type littermates (4 months n = 1; 20 months n = 1) were sacrificed by CO_2 inhalation and perfused transcardially with 0.9 % saline. Organs (brain, duodenum, heart, intestines, kidney, liver, spleen and stomach) were collected, snap frozen and stored at -70 °C.

RNA isolation

Organs were weighed, adjusted in size if exceeding the recommended weight limit and homogenized at 5,000 rpm using a Precellys homogenizer (Bertin Technologies S.A.S, Montigny-le-Bretonneux, France) and ceramic mix beads of 1.4 mm and 2.8 mm for 20 s to 40 s. Total RNA extraction was performed using SV Total RNA Isolation Systems (Promega Corporation, Madison, WI, USA) according to the manufacturer's instructions with minor adjustments. All centrifugation steps were conducted at 13,000 rpm. The RNA was released from the membrane by centrifugation twice at 14,800 rpm with 20 µl of nuclease-free water. Concentrations of the isolated RNA samples were measured by spectrophotometry using a NanoDrop 2000 (Thermo Fisher Scientific, Wilmington, DE, USA). All samples had an A260/280 ratio between 1.9 and 2.2. Samples with an A260/230 ratio under 1.6 were further post-processed according to the manufacturer's instructions. For further information, see **Suppl. Table 1**. The quality of extracted RNA was visualized with formaldehyde gel electrophoresis. All samples were diluted to a final concentration of 10 ng/µl using nuclease-free water and stored at -70 °C until further quantification.

The *mPgpep1* gene was cloned into a pET-28a(+) cloning vector (Gene Universal Inc., Newark, NJ, USA). For the purification of the plasmid, the QIAprep Spin Miniprep Kit (QIAGEN, Hilden, Germany) was used according to the manufacturer's protocol. The plasmid was eluted in 60 µl followed by another elution step with 20 µl. Concentration was measured using a Nanodrop 2000 (Thermo Fisher Scientific, Wilmington, DE, USA) and stored in aliquots at -20 °C.

RT-qPCR for Pgpep-1

An absolute RT-qPCR was performed for the quantification of the *Pgpep1* expression (NM_023217.4) in different tissues and organs. Primers were designed using Primer3 [88–90] and Primer-BLAST (National Center for Biotechnology Information (NCBI), National Library of Medicine (NIH), Bethesda, MD, USA) [91] and verified for specificity to *Pgpep1* via Primer-BLAST analysis (forward: CGGAAGGCGGTAGTGGTAAC; reverse: AACATGCACTACGAGCTGGG). To prevent genomic DNA contamination, primers were designed to span exon-intron junctions (**Suppl. Table 1**). Primer specificity was confirmed with agarose gel electrophoresis and melting curve analysis (**Extended Data Fig. 4**).

A one-step RT-PCR Kit (QIAGEN, Hilden, Germany) was used according to the manufacturer's instructions with minor adjustments. Each 10 µl RT-qPCR mix contained 0.6 µl of each 10 µM forward and reverse primer, 0.4 µl dNTP Mix (containing 10 nM of each dNTP), 0.4 µl QIAGEN OneStep RT-PCR Enzyme Mix, 2 µl 5xQIAGEN OneStep RT-PCR Buffer, 0.5 µl SYBR Green, 0.5 µl Dimethyl sulfoxide and 2 µl of 10 ng/µl RNA sample. The cycling protocol performed in a Rotor-Gene Q (QIAGEN, Hilden, Germany) included reverse transcription (50 °C, 30 min), initial activation (95 °C, 15 min), 40 cycles of denaturation (94 °C, 1 min), annealing (60 °C,

1 min) and extension (72 °C, 1 min) with fluorescence measurement at 84 °C. A final extension was carried out at 72 °C for 10 min, followed by melting curve analysis and agarose gel electrophoresis to verify amplification specificity. A standard curve of the target plasmid was prepared, starting with a 10-fold dilution followed by 5-fold dilutions (**Extended Data Fig. 4**). For each instrumental run, the standard curve ranged from 1.54 x 10^5 to 6.16 x 10^2 copies per reaction ($R^2 \geq 0.98$). To obtain individual Cq values, each sample was measured in three technical replicates. Outlier Cq values were removed and at least two duplicate Cq values were retained for analysis. For further information, see **Suppl. Table 1**. The cDNA copy numbers, reflecting the starting RNA concentration of the samples, were calculated using the equation for standard curve calculation provided by the Rotor-Gene Software (version 2.2.2).

Cell culture experiments and toxicity assays

Toxicity assays of (aggregated) Aβ(1-40/42), Aβ(pGlu3-40/42) and Aβ(4-40/42) on GT1-7 cells were performed according to Bluhm et al. [92] In short, GT1-7 cells were grown in Dulbecco's modified Eagle's medium (DMEM) F12 (Gibco, Thermo Fisher Scientific, Wilmington, DE, USA) supplemented with 10 % fetal bovine serum (FBS) at 37 °C and 5 % CO_2. To induce differentiation toward a differentiated neuronal phenotype, 1.25 x 10^4 cells/well were seeded in a transparent 96-well plate, and the medium was changed to DMEM F12 supplemented with 2 % FBS for three to five days. After the differentiation for three to five days, the medium of the cells was changed to Opti-MEM reduced serum medium (Gibco, Thermo Fisher Scientific, Wilmington, DE, USA) for measurements. MitoTracker Deep Red FM (M22426; Invitrogen, Waltham, MA, USA) was added to the GT1-7 cells according to the manufacturer's protocol and the cells were exposed to different Aβ variants and aggregation states (freshly prepared or pre-aggregated for at least 24 h) and cultured at 37 °C in a humidified atmosphere containing 5 % CO_2 for 24 h. Over the course of 24 h, GT1-7 cells were continuously imaged using a Celldiscoverer 7 (Carl Zeiss Microscopy GmbH, Oberkochen, Germany) equipped with the AxioCam506 and a Colibri2 light source. Cells were imaged using bright field acquisition. In parallel, MitoTracker-labeled active mitochondria were measured at 625 nm and used as an indicator of neuronal viability.

WST-8 assay was performed 24 h after adding the Aβ peptides. 2-(2-methoxy-4-nitrophenyl)-3-(4-nitrophenyl)-5-(2,4-disulfophenyl)-2H-tetrazolium (WST-8, monosodium salt; Manchester Organics, Runcorn, UK) was used at 5 mM in 150 mM NaCl and supplemented with 200 µM 1-methoxy-5-methylphenazinium methylsulfate (1-Methoxy-PMS; Dojindo Molecular Technologies, Munich, Germany). Next, 10 µl WST-8/1-Methoxy-PMS mix was added to 100 µl medium in 96-well plates [93]. The resulting soluble formazan dye formed within 90 min depending on cell density and absorbance was read at 450 nm using a Mithras LB 940 plate reader (Berthold Technologies GmbH & Co.KG, Bad Wildbad, Germany). Fluorescence

intensities of MitoTracker at 24 h or WST-8 intensity were compared using one-way ANOVA followed by Bonferroni correction. Differences between groups were considered statistically significant for p values < 0.05.

Table 1: Primary and secondary antibodies for detection of different epitopes by immunohistochemistry (IHC) and immunofluorescence (IF)

Antibodies			Mouse		Human	
Antibody (Clone/ catalog number; Concentration [mg/ml])	**Company / Supplier**	**Host**	**IHC**	**IF**	**IHC**	**IF**
Aβ (MOAB-2) (6C3/ 11610)	Cayman Chemical (Ann Arbor, MI, USA)	Mouse (IgG2b)	-	1:1,000	-	1:1,000
Aβ(4-x) (58-1; 1.00)	University Medical Center Göttingen (Göttingen, Germany)	Rabbit	1:2,000	1:1,000	1:2,000	1:1,000
Aβ(pGlu3-x) (J8; 1.00)	Fraunhofer IZI (Halle, Germany)	Mouse (IgG1/ IgG2a)	1:200	1:100	1:200	1:100
Calbindin (McAB 300)	SWANT (Burgdorf, Switzerland)	Mouse (IgG1)	-	1:1,000	-	-
Calreticulin (ab14234)	abcam (Cambridge, UK)	Chicken	-	1:100	-	-
CCL2 (AF-479)	R&D Systems, Bio-Techne Corporation, (Minneapolis, MN, USA)	Goat	1:200	-	-	-
GFAP (PA5-18598)	Invitrogen (Waltham, MA, USA)	Goat	-	1:10,000	-	-
Iba1 (Gp311H9/ 234308)	Synaptic Systems (Göttingen, Germany)	Guinea pig	-	1:200	-	-
Parvalbumin (195004)	Synaptic Systems (Göttingen, Germany)	Guinea pig	-	1:1,400	-	-
pGlu-TRH (PAB13482)	Abnova (Taipei City, Taiwan)	Rabbit	1:50	-	-	-
PGP-1 (HPA035368)	Sigma-Aldrich, Merck KGaA (Darmstadt, Germany)	Rabbit	1:600	1:200-1:300		-
Somatostatin (sc-7819)	Santa Cruz Biotechnology, Inc. (Dallas, TX, USA)	goat	-	1:100	-	-
Syntaxin 6 (3D10/ ab12370)	abcam (Cambridge, UK)	Mouse	-	1:100	-	-

Table 2: Human brain tissue of the temporal cortex used for immunohistochemical and immunofluorescent labelings as well as immunoassay and mass spectrometric analyses

	Case #	Age [years]	PMI [h]	Gender f / m	Brain weight [g]	CAA yes / no	Braak score	Thal phase	APOE genotype	MMSE score	CERAD criteria	NIA-AA criteria	Unified LB stage
AD	AD1	76	3.08	f	862	yes	V	n.a.	3/3	6	definite AD	high	0
	AD2	92	3.73	f	1,110	yes	VI	5	3/4	7	definite AD	high	0
	AD3	75	3.83	m	1,070	yes	V	5	3/4	3	definite AD	high	0
	AD4	77	3.62	m	1,180	yes	VI	5	3/4	10	definite AD	high	0
	AD5	83	4	m	1,184	yes	V	5	3/4	14	definite AD	high	0
	AD6	83	3.62	f	1,052	yes	V	5	3/3	17	definite AD	high	0
	AD7	84	3.33	f	1,142	yes	VI	5	3/3	24	definite AD	high	0
	AD8	83	3.58	m	1,105	yes	V	5	2/4	3	definite AD	high	0
	AD9	75	2.97	m	1,251	yes	V	5	3/4	25	definite AD	high	0
	AD10	82	4	f	1,098	yes	VI	5	3/3	19	definite AD	high	0
	AD11	77	48	f	-	-	V-VI	-	-	-	-	-	-
	AD12	77	34	f	1,070	-	V-VI	-	-	-	-	-	-
	AD13	69	40	m	1,370	-	V-VI	-	-	-	-	-	-
	AD14	86	9	m	1,300	-	VI	-	-	-	-	-	-
	AD15	76	32	m	1,310	-	V-VI	-	-	-	-	-	-
	AD16	83	48	f	1,000	-	V-VI	-	-	-	-	-	-
	AD17	81	18	f	1,150	-	V-VI	-	-	-	-	-	-

PMI *post mortem* interval; ***f*** female; ***m*** male; ***CAA*** Cerebral Amyloid Angiopathy; ***Braak score*** Braak neurofibrillary stage I - VI [78]; ***Thal phase*** Thal amyloid staging with phases 0 (A0), 1 (A1), 2 (A1), 3 (A2), 4 (A3) and 5 (A3) [94,95]; ***APOE genotype*** apolipoprotein E genotype; ***MMSE score*** last Mini Mental State Examination score before death; ***CERAD criteria*** diagnosis of AD based on criteria of the Consortium to establish a registry for AD; ***NIA-AA criteria*** diagnosis of AD based on criteria of the National Institute on Aging - Alzheimer's Association; ***Unified LB stage*** unified staging system for Lewy body disorders with stage 0 (no Lewy bodies), I (olfactory bulb only), IIa (brainstem predominant), IIb (limbic predominant), III (brainstem and limbic), IV (neocortical) [96]; **empty (-)** n.a.

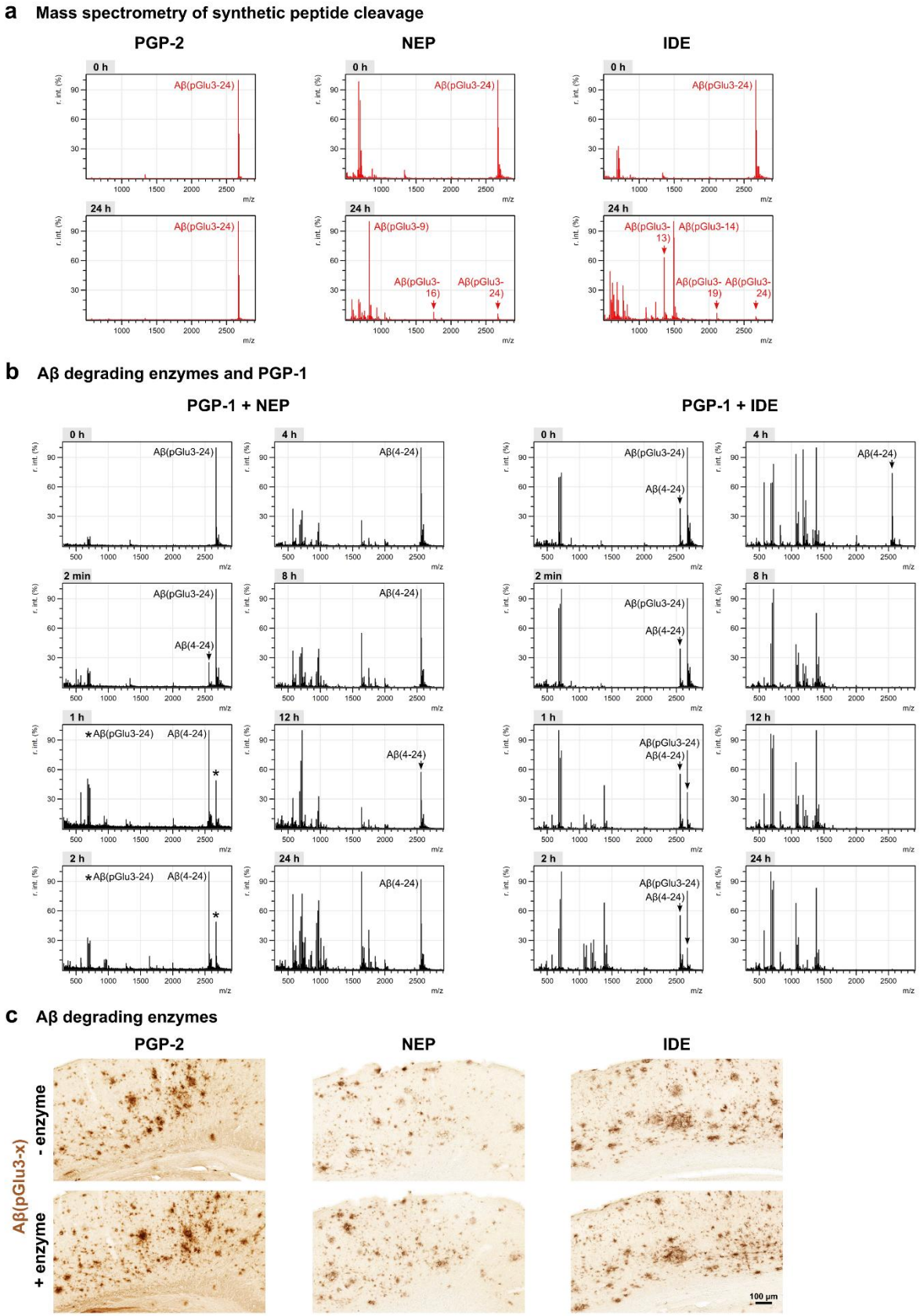
Table 3: Enzymes

Enzyme	Company	Concentration [mg/ml]	Specific activity [pmol/min/µg]
IDE	R&D Systems, Bio-Techne Corporation (Minneapolis, MN, USA)	0.44	>1000
NEP		0.44	>1500
PGP-1		0.44	>9500
PGP-2		0.51	>130

Table 4: Synthetic standard peptides for mass spectrometry and aggregation analyses

Peptide	Sequence	Origin
Aβ(pGlu3-24) (MH1+ 2671.269)	(pE)FRHDSGYEVHHQKLVFFAEDV-OH	University of Leipzig, Medical Faculty, Core Unit Peptide (Leipzig, Germany)
Aβ(1-40)	H-DAEFRHDSGYEVHHQKLVFFAEDVGSNKGAIIGLMVGGVV-OH	Department of Pathology, New York University School of Medicine (New York, NY, USA)
Aβ(1-42)	H-DAEFRHDSGYEVHHQKLVFFAEDVGSNKGAIIGLMVGGVVIA-OH	
Aβ(4-40)	H-FRHDSGYEVHHQKLVFFAEDVGSNKGAIIGLMVGGVV-OH	
Aβ(4-42)	H-FRHDSGYEVHHQKLVFFAEDVGSNKGAIIGLMVGGVVIA-OH	
Aβ(pGlu3-40)	(pE)FRHDSGYEVHHQKLVFFAEDVGSNKGAIIGLMVGGVV-OH	
Aβ(pGlu3-42)	(pE)FRHDSGYEVHHQKLVFFAEDVGSNKGAIIGLMVGGVVIA-OH	

Extended Data figures

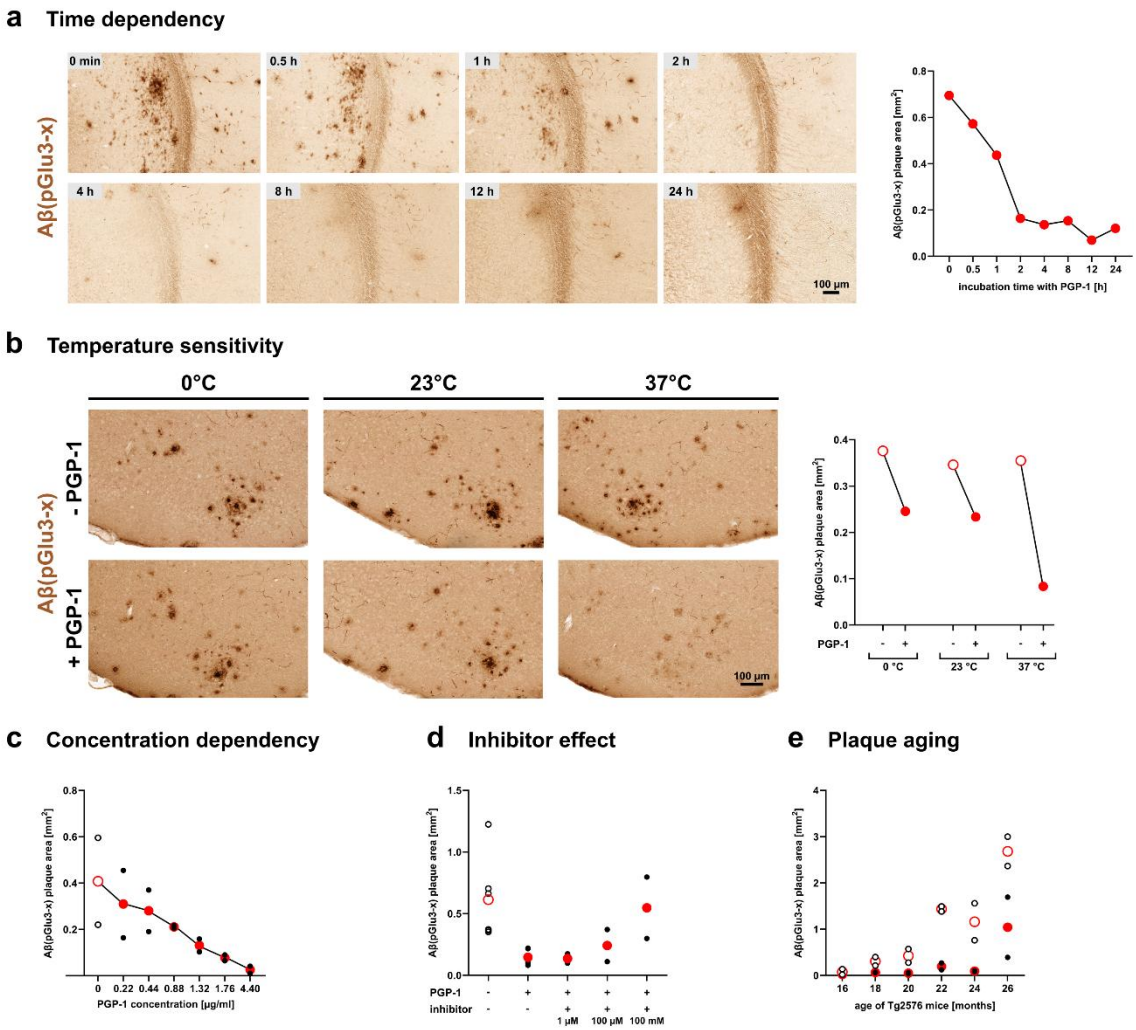


Extended Data Fig. 1: Enzymatic effect of PGP-2, NEP and IDE on Aβ(pGlu3-x). a) Enzymatic effects of PGP-2, NEP and IDE on the synthetic Aβ(pGlu3-24) peptide monitored by mass spectrometric analysis for different periods of time as indicated. PGP-2 did not degrade Aβ(pGlu3-24). NEP and IDE generated C-terminal cleavage products but left the pGlu-terminus intact. **b)** Time-dependent mass spectrometric analysis

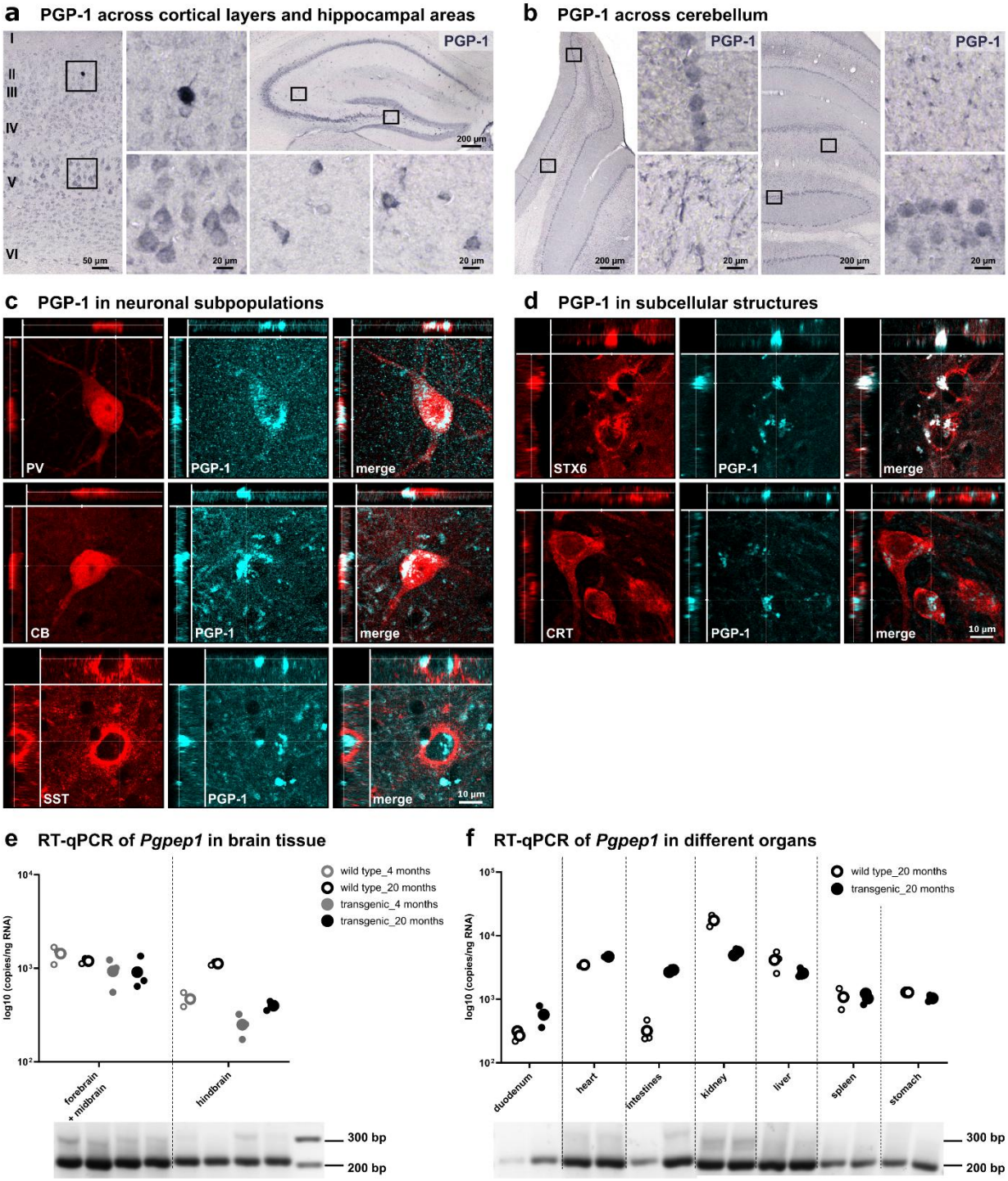
of Aβ(pGlu3-24) and its cleavage products after incubation with PGP-1 and NEP or PGP-1 and IDE, respectively. The different periods of time are indicated. **c)** The enzymes PGP-2, NEP and IDE did not reduce the Aβ(pGlu3-x) immunoreactivity in Tg2576 mouse brain sections after incubation at 37 °C for 24 h. Scale bars apply to all micrographs in the respective panel.

Extended Data Table 1: Cleavage products after incubation of Aβ(pGlu3-24) with PGP-1, NEP, IDE, PGP-1 + NEP or PGP-1 + IDE, respectively. After incubation of Aβ(pGlu3-24) with different enzymes for 0 h and 24 h, fragments of Aβ(pGlu3-24) were detected using MALDI mass spectrometry. Listed are the sequences of the fragments, their experimental m/z ratio (m/z exp.) and calculated m/z ratio (m/z calc.).

Enzyme	Time	Fragment	Sequence	m/z exp.	m/z calc.
PGP-2	0 h	3-24	pE F R H D S G Y E V H H Q K L V F F A E D V	2671.266	2671.269
	0 h	3-24	pE F R H D S G Y E V H H Q K L V F F A E D V	2671.313	2671.269
NEP	0 h	3-24	pE F R H D S G Y E V H H Q K L V F F A E D V	2671.167	2671.269
	24 h	3-24	pE F R H D S G Y E V H H Q K L V F F A E D V	2671.239	2671.269
		3-17	pE F R H D S G Y E V H H Q K L	1863.835	1863.889
		3-16	pE F R H D S G Y E V H H Q K	1750.754	1750.804
		3-11	pE F R H D S G Y E	1121.431	1121.465
		10-17	Y E V H H Q K L	1053.513	1053.548
		3-9	pE F R H D S G	829.333	829.359
IDE	0 h	3-24	pE F R H D S G Y E V H H Q K L V F F A E D V	2671.248	2671.269
	24 h	3-24	pE F R H D S G Y E V H H Q K L V F F A E D V	2671.259	2671.269
		3-19	pE F R H D S G Y E V H H Q K L V F	2110.016	2110.025
		3-14	pE F R H D S G Y E V H H	1494.645	1494.651
		3-13	pE F R H D S G Y E V H	1357.589	1357.5893
		5-14	R H D S G Y E V H H	1236.545	1236.55
		5-13	R H D S G Y E V H	1099.487	1099.492
		14-19	H Q K L V F	771.446	771.451
		3-7	pE F R H D	685.305	685.305
		20-24	F A E D V	580.268	580.261
PGP-1 + NEP	0 h	3-24	pE F R H D S G Y E V H H Q K L V F F A E D V	2671.231	2671.269
	24 h	4-24	F R H D S G Y E V H H Q K L V F F A E D V	2560.422	2560.237
		4-19 or 5-20	F R H D S G Y E V H H Q K L V F F	1999.137	1998.993
		4-18 or 5-19	F R H D S G Y E V H H Q K L V F	1852.058	1851.925
		4-17	F R H D S G Y E V H H Q K L	1752.981	1752.856
		4-16	F R H D S G Y E V H H Q K	1639.889	1639.772
		10-17	Y E V H H Q K L	1053.615	1053.548
		4-11	F R H D S G Y E	1010.5	1010.433
		17-24	L V F F A E D V	939.538	939.482
		18-24	V F F A E D V	826.448	826.398
		18-23 or 19-24	V F F A E D V	727.377	727.33
		4-9	F R H D S G	718.372	718.327
		20-24	F A E D V	580.309	580.261
		4-7	F R H D	574.32	574.273
		17-19	L V F	378.313	378.239
PGP-1 + IDE	0 h	3-24	pE F R H D S G Y E V H H Q K L V F F A E D V	2671.316	2671.269
	24 h	4-15	F R H D S G Y E V H H Q	1511.692	1511.677
		8-19	S G Y E V H H Q K L V F	1443.566	1443.738
		4-14	F R H D S G Y E V H H	1383.632	1383.619
		14-24	H Q K L V F F A E D V	1332.696	1332.695
		4-13	F R H D S G Y E V H	1246.571	1246.56
		15-24	pE K L V F F A E D V	1178.614	1178.611
		16-24	K L V F F A E D V	1067.584	1067.577
		8-14	S G Y E V H H	828.369	828.363
		10-14	Y E V H H	684.315	684.31
		4-7	F R H D	574.284	574.273
		16-19	K L V F	506.349	506.334
		4-6	F R H	459.265	459.246



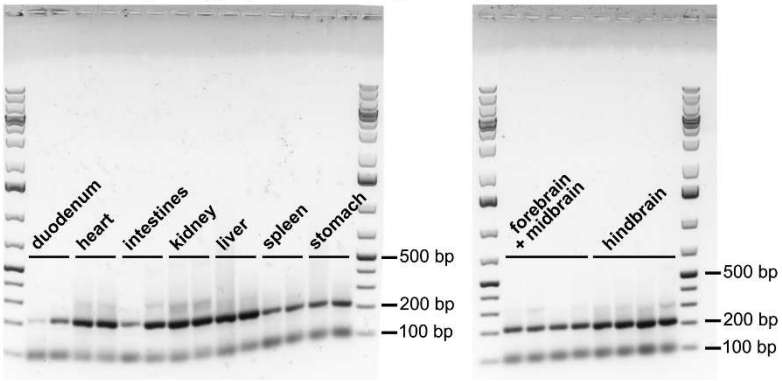
Extended Data Fig. 2: Enzymatic characteristics of Aβ(pGlu3-x) degradation by PGP-1. a) In brain sections of hAPP-transgenic mice Tg2576 with Aβ(pGlu3-x) plaque pathology, a time-dependent reduction of Aβ(pGlu3-x) immunoreactivity after incubation with PGP-1 was observed (n = 1). **b)** The reduction of Aβ(pGlu3-x) immunoreactivity after incubation with PGP-1 is temperature sensitive (n = 1), **c)** dependent on the PGP-1 concentration applied (n = 1) and can be **d)** prevented by the PGP-1 inhibitor 2-pyrrolidone (n = 1). **e)** The reduction of the Aβ(pGlu3-x) plaque load in aged Tg2576 mice is as effective as in younger Tg2576 mice (n = 1 for each age). For **c) – e)**, large red dots/ circles show the mean of the two technical replicates (small black dots/ circles). Circles represent data in the absence of PGP-1, dots represent data collected in the presence of PGP-1 (n = 1). Scale bars apply to all micrographs in the respective panel.



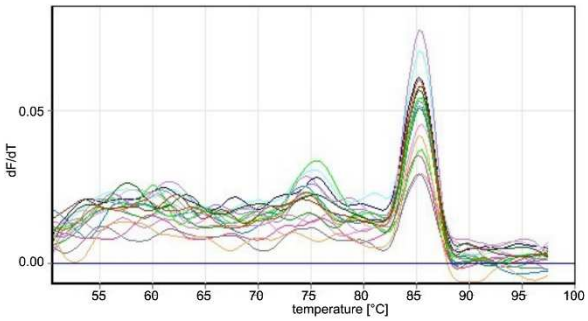
Extended Data Fig. 3: Expression of *Pgpep1* mRNA and PGP-1 protein in brain and mouse peripheral organs. a) Immunohistochemistry for PGP-1 in mouse brain revealed a moderate labeling intensity and cytoplasmic localization in neocortical and hippocampal neurons. Individual neurons displayed a strong PGP-1 immunoreactivity. **b)** In cerebellum, a moderate immunohistochemical PGP-1 labeling was shown in Purkinje cells. **c)** PGP-1 was found to be expressed by parvalbumin (PV)-, calbindin (CB)- and somatostatin (SST)-immunoreactive interneurons as shown for 18 months old Tg2576 mouse brain, and **d)** to be co-localized to the Golgi marker syntaxin-6 (STX-6). PGP-1 was not co-localized with the endoplasmic reticulum marker calreticulin (CRT). Similar expression patterns were observed for wild type mouse brain. **e)** In forebrain and midbrain tissue, RT-qPCR identified similar *Pgpep1* copy numbers for young and aged mice of wild type and hAPP-transgenic genotype. In hindbrain structures, higher *Pgpep1* copy numbers were detected in aged mice of both genotypes, compared to young mice. In addition, aged Tg2576 mice displayed lower *Pgpep1* copy numbers than their wild type littermates. Wild type_4 months: n = 1; wild type_20 months: n = 1; transgenic_4 months: n = 1; transgenic_20 months: n = 1 animal was analyzed. Large dots/ circles show the mean of the three technical replicates (small circles/ dots) of each organ. **f)** RT-

qPCR identified highest *Pgpep1* transcript copy numbers in kidney, liver, spleen and heart and lower copy numbers in stomach, intestine and duodenum of 20-month-old B6SJL mice. There were no differences between wild type and hAPP-transgenic Tg2576 mice except for higher *Pgpep1* copy numbers in intestine of transgenic mice. Wild type_20 months: n = 1; transgenic_20 months: n = 1 animal was analyzed. Large dots/ circles show the mean of the three technical replicates (small circles/ dots) of each organ. Scale bars apply to all micrographs in the respective panel.

a **Specificity of *Pgpep1* Primer in agarose gel electrophoresis**



b **Specificity of *Pgpep1* Primer in melting curve analysis**



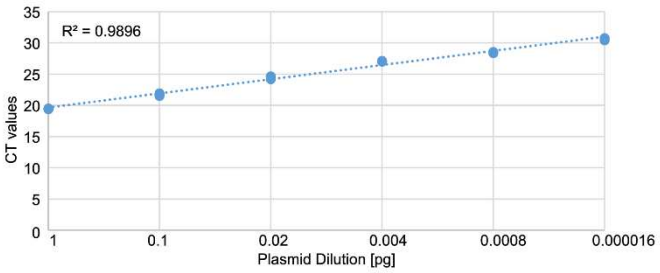
c **Dynamic Range**

Quantitation Information	
Threshold	0.01
Left Threshold	1.000
Standard Curve Imported	No
Standard Curve (1)	conc= 10^(-0.330*CT + 11.342)
Standard Curve (2)	CT = -3.034*log(conc) + 34.412
Reaction efficiency (*)	(* = 10^(-1/m) - 1) 1.13602
M	-303.393
B	3.441.192
R Value	0.99477
R^2 Value	0.98957
Start normalising from cycle	100%
Noise Slope Correction	Yes
No Template Control Threshold	0%
Reaction Efficiency Threshold	Disabled
Normalisation Method	Dynamic Tube Normalisation
Digital Filter	Light

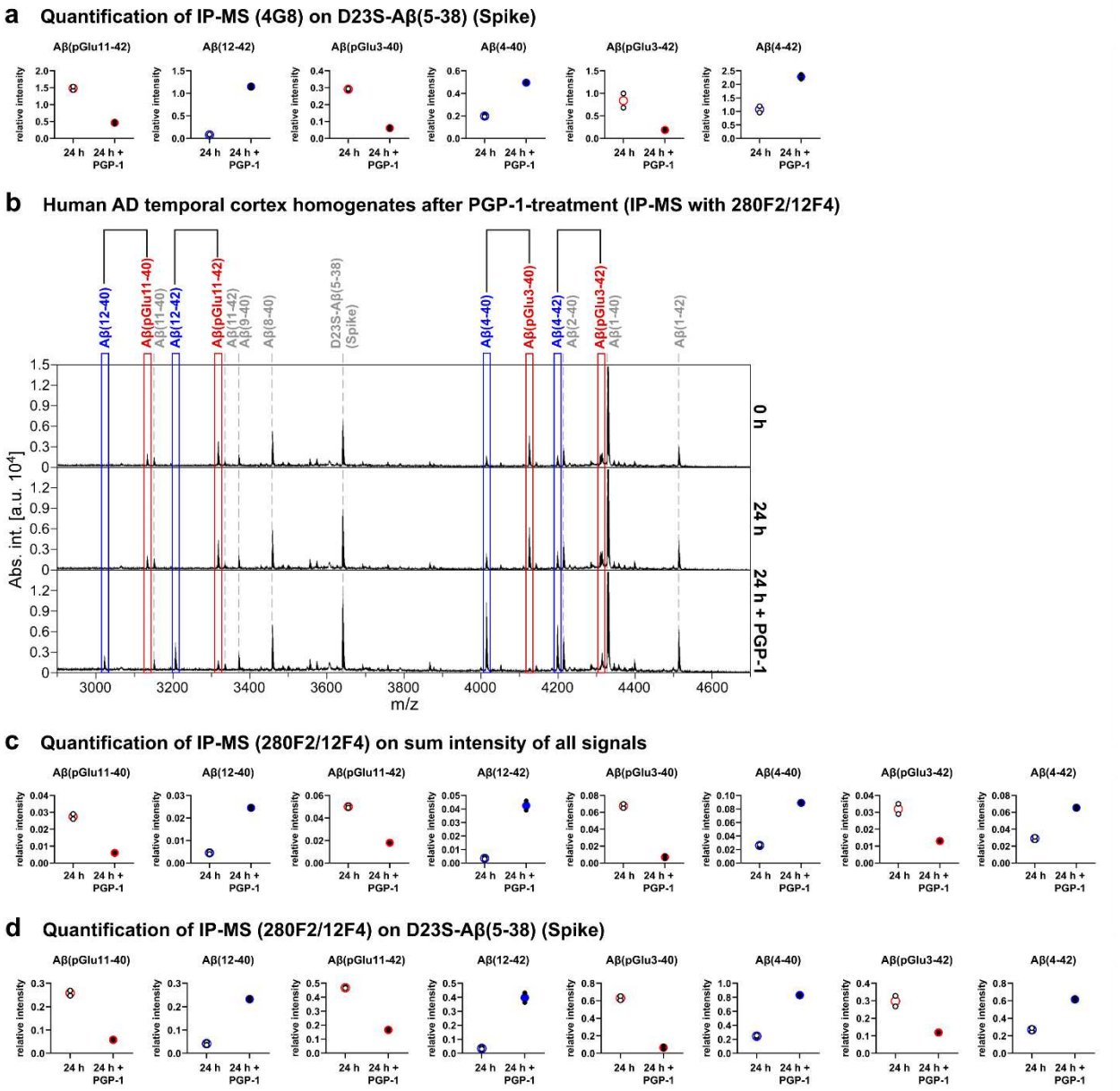
d **Standard Curve of Dynamic Range**

Plasmid Dilution	CT	SD
PGPEP1 _Plasmid_1 pg	19.52	0.06
PGPEP1 _Plasmid_1 pg	19.39	
PGPEP1 _Plasmid_1 pg	19.41	
PGPEP1 _Plasmid_0.1 pg	21.91	0.16
PGPEP1 _Plasmid_0.1 pg	21.51	
PGPEP1 _Plasmid_0.1 pg	21.73	
PGPEP1 _Plasmid_0.02 pg	24.63	0.21
PGPEP1 _Plasmid_0.02 pg	24.17	
PGPEP1 _Plasmid_0.02 pg	24.61	
PGPEP1 _Plasmid_0.004 pg	27.00	0.07
PGPEP1 _Plasmid_0.004 pg	27.14	
PGPEP1 _Plasmid_0.004 pg	26.98	
PGPEP1 _Plasmid_0.0008 pg	28.36	0.10
PGPEP1 _Plasmid_0.0008 pg	28.56	
PGPEP1 _Plasmid_0.0008 pg	*29.54	
PGPEP1 _Plasmid_0.00016 pg	*30.80	0.18
PGPEP1 _Plasmid_0.00016 pg	30.76	
PGPEP1 _Plasmid_0.00016 pg	30.40	

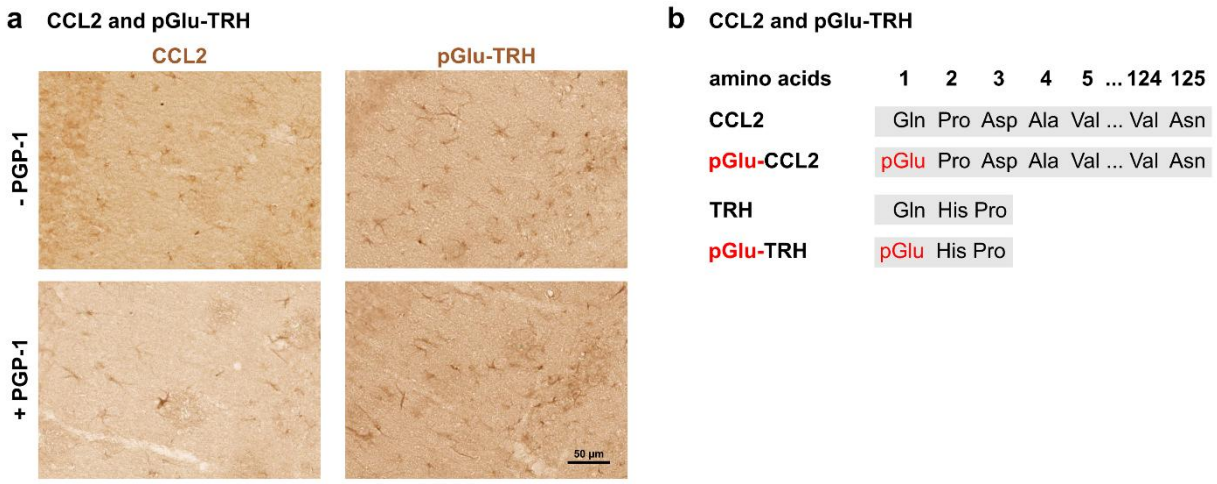
* : value not inluded in analysis



Extended Data Fig. 4: Verification of RT-qPCR experiments. a) Agarose gel electrophoresis showing the specific *Pgpep1* amplicon at 207 bp. **b)** Representative melting curve analysis of a selection of organs demonstrating a single peak at 85.3 °C, confirming amplification specificity. **c)** Dynamic range of *Pgpep1* plasmid detection from 1 pg to 0.00016 pg. **d)** Standard curve generated from the serial dilution corresponding to the dynamic range of *Pgpep1*.



Extended Data Fig. 5: Detection of Aβ peptides in PGP-1-treated human brain homogenates by IP-MS. a) Quantification of selected Aβ signals relative to the intensity of the signal of the spike peptide D23S-Aβ(5-38). IP-MS was performed with 4G8; see mass spectra in Fig. 3e. **b)** Mass spectra showing the changes in abundance of different Aβ peptides in human brain homogenates (pooled sample of AD1 to AD10) after incubation with PGP-1 at 37 °C for 24 h. IP-MS was performed with a mixture of 280F2/12F4. The substrate/ product pairs are boxed in red and blue, respectively. One representative mass spectrum out of two per condition is shown. **c-d)** Quantification of selected Aβ signals relative to the sum intensity of all signals in the mass range 2900-5000 m/z (except for the signal of the spike peptide D23S-Aβ(5-38)) (**c**) or relative to the intensity of the signal of the spike peptide D23S-Aβ(5-38) alone (**d**). Large red or blue dots/ circles show the mean of the two technical replicates (small black dots/ circles). Quantification demonstrates the degradation of Aβ(pGlu3-40/42) and Aβ(pGlu11-40/42) variants present in human brain tissue homogenates and the corresponding increase in the respective truncated Aβ variants. All other Aβ variants detected by mass spectrometry, such as Aβ1-40 and Aβ1-42, remained unaffected by PGP-1.



Extended Data Fig. 6: Physiological PGP-1 substrates. a) The enzyme PGP-1 did not reduce pGlu-TRH and CCL2 immunoreactivity in 5xFAD mouse brain sections after incubation at 37 °C for 24 h. **b)** Amino acid sequences of (pGlu-)CCL2 and (pGlu-)TRH. Scale bar applies to all micrographs in the panel.

List of abbreviations

Aβ	amyloid β
AD	Alzheimer's disease
APOE	apolipoprotein E
APP	amyloid precursor protein
ARIA	amyloid-related imaging abnormality
BSA	bovine serum albumin
CAA	cerebral amyloid angiopathy
CHCA	α-cyano-4-hydroxycinnamic acid
DAB	3,3'-diaminobenzidine
DDM	n-dodecyl-β-d-maltoside
DHB	2,5-dihydroxybenzoic acid
FA	formic acid
GdmCl	guanidinium chloride
HFIP	hexafluoroisopropanol, 1,1,1,3,3,3-hexafluoro-2-propanol
HRP	horseradish peroxidase
IDE	insulin-degrading enzyme
IP	immunoprecipitation
LB stage	Unified Staging System for Lewy Body Disorders
MMSE	Mini Mental State Examination
MS	mass spectrometry
NEP	neutral endopeptidase, neprilysin
NTM	nonyl-β-d-thiomaltoside
PBS	phosphate-buffered saline
PBS-T	PBS containing 0.02% Tween 20
PGP-1	pyroglutamyl-peptidase 1 (enzyme)
Pgpep1	pyroglutamyl-peptidase 1 (murine gene)
PGP-2	pyroglutamyl-peptidase 2 (enzyme), thyrotropin-releasing hormone-degrading ectoenzyme
PMI	*post mortem* interval
PSEN1	presenilin-1
PTM	post-translational modifications
QC	glutaminyl cyclase
RT-qPCR	reverse transcription quantitative PCR
TBS	Tris-buffered saline
TEM	Transmission electron microscopy
TFA	trifluoroacetic acid
ThT	thioflavin T
TMB	3,3′,5,5′-Tetramethylbenzidin
WST-8	2-(2-methoxy-4-nitrophenyl)-3-(4-nitrophenyl)-5-(2,4-disulfophenyl)-2H-tetrazolium

DECLARATIONS

Availability of data and materials

The datasets used and analyzed during the current study are available from the corresponding author on reasonable request.

Competing interests

The authors declare that they have no competing interests.

Consent for publication

All the authors have approved publication.

Authors' contributions

Sa.S. designed the study, performed histological and biochemical tissue processing, enzyme assays for histological and mass spectrometric analyses, data analysis and visualization and was a major contributor in manuscript writing.
C.H. designed the study, performed histological tissue processing, performed protein aggregation and cell culture assays, data analysis and visualization.
C.M. performed histological tissue processing, RT-qPCR data acquisition, data analysis and visualization.
T.L. performed IP-MS data acquisition and data analysis.
M.N. provided experimental tools, supervised mass spectrometric analyses and gave scientific advice.
A.K.K. performed biochemical tissue processing and gave scientific advice.
M.S. performed histological tissue processing, enzyme assays for histological analyses and data visualization.
M.F. provided experimental tools and gave scientific advice.
M.H.R. provided scientific advice.
M.H. provided scientific advice.
D.A. designed and supervised stereotactic injections.
R.R. designed and supervised stereotactic injections.
M.P. designed and supervised stereotactic injections.
A.S. provided experimental tools and gave scientific advice.
H.C. gave scientific advice.
G.E.S. helped select human subject cases appropriate for the project and performed clinico-pathological classification of human subjects.
T.G.B. helped select human subject cases appropriate for the project and performed clinico-pathological classification of human subjects.
J.G. provided experimental tools and gave scientific advice.
M.M. supervised imaging via transmission electron microscopy and provided scientific advice.
J.S. gave scientific advice.
O.J. provided experimental tools, designed and supervised biochemical analyses, gave scientific advice on interpretation of data and contributed to manuscript writing.
O.W. provided experimental tools, designed and supervised biochemical analyses, gave scientific advice on interpretation of data and contributed to manuscript writing.
St.S. gave scientific advice.
S.R. initiated, designed and supervised the study and was a major contributor in writing the manuscript.

References

1. Aisen, P. *et al.* The case for regulatory approval of amyloid-lowering immunotherapies in Alzheimer's disease based on clearcut biomarker evidence. *Alzheimer's & dementia : the journal of the Alzheimer's Association* **21,** e14342; 10.1002/alz.14342 (2025).
2. Heneka, M. T., Morgan, D. & Jessen, F. Passive anti-amyloid β immunotherapy in Alzheimer's disease-opportunities and challenges. *Lancet* **404,** 2198–2208; 10.1016/S0140-6736(24)01883-X (2024).
3. Iwata, N. *et al.* Identification of the major Abeta1-42-degrading catabolic pathway in brain parenchyma: suppression leads to biochemical and pathological deposition. *Nat Med* **6,** 143–150; 10.1038/72237 (2000).
4. Iwata, N. *et al.* Metabolic regulation of brain Abeta by neprilysin. *Science* **292,** 1550–1552; 10.1126/science.1059946 (2001).
5. Iwata, N., Higuchi, M. & Saido, T. C. Metabolism of amyloid-beta peptide and Alzheimer's disease. *Pharmacol Ther* **108,** 129–148; 10.1016/j.pharmthera.2005.03.010 (2005).
6. Qiu, W. Q. *et al.* Insulin-degrading enzyme regulates extracellular levels of amyloid beta-protein by degradation. *J Biol Chem* **273,** 32730–32738; 10.1074/jbc.273.49.32730 (1998).
7. Fu, H., Liu, B., Li, L. & Lemere, C. A. Microglia Do Not Take Up Soluble Amyloid-beta Peptides, But Partially Degrade Them by Secreting Insulin-degrading Enzyme. *Neuroscience* **443,** 30–43; 10.1016/j.neuroscience.2020.07.020 (2020).
8. Tcw, J. & Goate, A. M. Genetics of β-Amyloid Precursor Protein in Alzheimer's Disease. *Cold Spring Harb Perspect Med* **7**; 10.1101/cshperspect.a024539 (2017).
9. Yang, X. *et al.* On the role of sidechain size and charge in the aggregation of Aβ42 with familial mutations. *Proc Natl Acad Sci U S A* **115,** E5849-E5858; 10.1073/pnas.1803539115 (2018).
10. Kummer, M. P. & Heneka, M. T. Truncated and modified amyloid-beta species. *Alzheimers Res Ther* **6,** 1–9; 10.1186/alzrt258 (2014).
11. Roher, A. E. *et al.* APP/Aβ structural diversity and Alzheimer's disease pathogenesis. *Neurochem Int* **110,** 1–13; 10.1016/j.neuint.2017.08.007 (2017).
12. Schrempel, S. *et al.* Identification of isoAsp7-Aβ as a major Aβ variant in Alzheimer's disease, dementia with Lewy bodies and vascular dementia. *Acta Neuropathol* **148,** 1–26; 10.1007/s00401-024-02824-9 (2024).
13. Saido, T. C. *et al.* Dominant and differential deposition of distinct beta-amyloid peptide species, Abeta N3(pE), in senile plaques. *Neuron* **14,** 457–466; 10.1016/0896-6273(95)90301-1 (1995).
14. Kuo, Y. M., Emmerling, M. R., Woods, A. S., Cotter, R. J. & Roher, A. E. Isolation, chemical characterization, and quantitation of Abeta 3-pyroglutamyl peptide from neuritic plaques and vascular amyloid deposits. *Biochem Biophys Res Commun* **237,** 188–191; 10.1006/bbrc.1997.7083 (1997).
15. Saido, T. C. Alzheimer's disease as proteolytic disorders: anabolism and catabolism of beta-amyloid. *Neurobiol Aging* **19,** S69-75; 10.1016/s0197-4580(98)00033-5 (1998).

16. Russo, C. *et al.* Pyroglutamate-modified amyloid beta-peptides--AbetaN3(pE)--strongly affect cultured neuron and astrocyte survival. *J Neurochem* **82,** 1480–1489; 10.1046/j.1471-4159.2002.01107.x (2002).

17. Iwata, N. *et al.* Metabolic resistance of Aβ3pE-42, a target epitope of the anti-Alzheimer therapeutic antibody, donanemab. *Life Sci Alliance* **7**; 10.26508/lsa.202402650 (2024).

18. Schlenzig, D. *et al.* Pyroglutamate formation influences solubility and amyloidogenicity of amyloid peptides. *Biochemistry* **48,** 7072–7078; 10.1021/bi900818a (2009).

19. Nussbaum, J. M. *et al.* Prion-like behaviour and tau-dependent cytotoxicity of pyroglutamylated amyloid-β. *Nature* **485,** 651–655; 10.1038/nature11060 (2012).

20. Schilling, S., Hoffmann, T., Manhart, S., Hoffmann, M. & Demuth, H. U. Glutaminyl cyclases unfold glutamyl cyclase activity under mild acid conditions. *FEBS Lett* **563**; 10.1016/S0014-5793(04)00300-X (2004).

21. Schilling, S. *et al.* Glutaminyl cyclase inhibition attenuates pyroglutamate Aβ and Alzheimer's disease–like pathology. *Nat Med* **14,** 1106–1111; 10.1038/nm.1872 (2008).

22. Alexandru, A. *et al.* Selective hippocampal neurodegeneration in transgenic mice expressing small amounts of truncated Aβ is induced by pyroglutamate-Aβ formation. *J Neurosci* **31,** 12790–12801; 10.1523/JNEUROSCI.1794-11.2011 (2011).

23. Hartlage-Rübsamen, M. *et al.* Glutaminyl cyclase contributes to the formation of focal and diffuse pyroglutamate (pGlu)-Aβ deposits in hippocampus via distinct cellular mechanisms. *Acta Neuropathol* **121,** 705–719; 10.1007/s00401-011-0806-2 (2011).

24. Morawski, M. *et al.* Glutaminyl cyclase in human cortex: correlation with (pGlu)-amyloid-β load and cognitive decline in Alzheimer's disease. *J Alzheimers Dis* **39,** 385–400; 10.3233/JAD-131535 (2014).

25. Jawhar, S., Wirths, O. & Bayer, T. A. Pyroglutamate amyloid-β (Aβ): a hatchet man in Alzheimer disease. *J Biol Chem* **286,** 38825–38832; 10.1074/jbc.R111.288308 (2011).

26. Bayer, T. A. Pyroglutamate Aβ cascade as drug target in Alzheimer's disease. *Mol Psychiatry* **27,** 1880–1885; 10.1038/s41380-021-01409-2 (2022).

27. Hoffmann, T. *et al.* Glutaminyl Cyclase Inhibitor PQ912 Improves Cognition in Mouse Models of Alzheimer's Disease-Studies on Relation to Effective Target Occupancy. *J Pharmacol Exp Ther* **362,** 119–130; 10.1124/jpet.117.240614 (2017).

28. Jawhar, S. *et al.* Overexpression of glutaminyl cyclase, the enzyme responsible for pyroglutamate A{beta} formation, induces behavioral deficits, and glutaminyl cyclase knock-out rescues the behavioral phenotype in 5XFAD mice. *J Biol Chem* **286,** 4454–4460; 10.1074/jbc.M110.185819 (2011).

29. Lues, I. *et al.* A phase 1 study to evaluate the safety and pharmacokinetics of PQ912, a glutaminyl cyclase inhibitor, in healthy subjects. *Alzheimers Dement (N Y)* **1,** 182–195; 10.1016/j.trci.2015.08.002 (2015).

30. Scheltens, P. *et al.* Safety, tolerability and efficacy of the glutaminyl cyclase inhibitor PQ912 in Alzheimer's disease: results of a randomized, double-blind, placebo-controlled phase 2a study. *Alzheimers Res Ther* **10,** 107; 10.1186/s13195-018-0431-6 (2018).

31. Vivoryon Therapeutics N.V. Vivoryon Therapeutics N.V. Provides Update on VIVIAD Phase 2b Study of Varoglutamstat in Early Alzheimer's Disease. Available at https://www.vivoryon.com/vivoryon-therapeutics-n-v-provides-update-on-viviad-phase-2b-study-of-varoglutamstat-in-early-alzheimers-disease/ (2024).

32. Frost, J. L. *et al.* Passive immunization against pyroglutamate-3 amyloid-β reduces plaque burden in Alzheimer-like transgenic mice: a pilot study. *Neurodegener Dis* **10,** 265–270; 10.1159/000335913 (2012).

33. Frost, J. L. *et al.* An anti-pyroglutamate-3 Aβ vaccine reduces plaques and improves cognition in APPswe/PS1ΔE9 mice. *Neurobiol Aging* **36,** 3187–3199; 10.1016/j.neurobiolaging.2015.08.021 (2015).

34. DeMattos, R. B. *et al.* A Plaque-Specific Antibody Clears Existing β-amyloid Plaques in Alzheimer's Disease Mice. *Neuron* **76,** 908–920; 10.1016/j.neuron.2012.10.029 (2012).

35. Lowe, S. L. *et al.* Donanemab (LY3002813) Phase 1b Study in Alzheimer's Disease: Rapid and Sustained Reduction of Brain Amyloid Measured by Florbetapir F18 Imaging. *J Prev Alzheimers Dis* **8,** 414–424; 10.14283/jpad.2021.56 (2021).

36. Gueorguieva, I. *et al.* Donanemab Population Pharmacokinetics, Amyloid Plaque Reduction, and Safety in Participants with Alzheimer's Disease. *Clin Pharmacol Ther* **113,** 1258–1267; 10.1002/cpt.2875 (2023).

37. Sims, J. R. *et al.* Donanemab in Early Symptomatic Alzheimer Disease: The TRAILBLAZER-ALZ 2 Randomized Clinical Trial. *JAMA* **330,** 512–527; 10.1001/jama.2023.13239 (2023).

38. Solopova, E. *et al.* Fatal iatrogenic cerebral β-amyloid-related arteritis in a woman treated with lecanemab for Alzheimer's disease. *Nat Commun* **14,** 8220; 10.1038/s41467-023-43933-5 (2023).

39. Hardy, J. & Schott, J. M. Identifying Genetic Risk for Amyloid-Related Imaging Abnormalities. *Neurology* **102,** e208096; 10.1212/WNL.0000000000208096 (2024).

40. Loeffler, D. A. Experimental approaches for altering the expression of Abeta-degrading enzymes. *J Neurochem* **164,** 725–763; 10.1111/jnc.15762 (2023).

41. Żukowska, J., Moss, S. J., Subramanian, V. & Acharya, K. R. Molecular basis of selective amyloid-β degrading enzymes in Alzheimer's disease. *FEBS J*; 10.1111/febs.16939 (2023).

42. Cummins, P. M. & O'Connor, B. Pyroglutamyl peptidase: an overview of the three known enzymatic forms. *Biochim Biophys Acta* **1429,** 1–17; 10.1016/s0167-4838(98)00248-9 (1998).

43. Charli, J.-L. *et al.* The Thyrotropin-Releasing Hormone-Degrading Ectoenzyme, a Therapeutic Target? *Front Pharmacol* **11**; 10.3389/fphar.2020.00640 (2020).

44. Hsiao, K. *et al.* Correlative memory deficits, Abeta elevation, and amyloid plaques in transgenic mice. *Science* **274,** 99–102; 10.1126/science.274.5284.99 (1996).

45. Mori, H., Takio, K., Ogawara, M. & Selkoe, D. J. Mass spectrometry of purified amyloid beta protein in Alzheimer's disease. *J Biol Chem* **267,** 17082–17086; 10.1016/S0021-9258(18)41896-0 (1992).

46. Masters, C. L. *et al.* Amyloid plaque core protein in Alzheimer disease and Down syndrome. *Proc Natl Acad Sci U S A* **82,** 4245–4249; 10.1073/pnas.82.12.4245 (1985).

47. Miller, D. L. *et al.* Peptide compositions of the cerebrovascular and senile plaque core amyloid deposits of Alzheimer's disease. *Arch Biochem Biophys* **301,** 41–52; 10.1006/abbi.1993.1112 (1993).

48. Walter, S. *et al.* The metalloprotease ADAMTS4 generates N-truncated Aβ4-x species and marks oligodendrocytes as a source of amyloidogenic peptides in Alzheimer's disease. *Acta Neuropathol* **137,** 239–257; 10.1007/s00401-018-1929-5 (2019).

49. Hornung, K. *et al.* N-Terminal Truncated Aβ4-42 Is a Substrate for Neprilysin Degradation in vitro and in vivo. *J Alzheimers Dis* **67**; 10.3233/JAD-181134 (2019).

50. Kemeh, M. M. & Lazo, N. D. Modulation of the Activity of the Insulin-Degrading Enzyme by Aβ Peptides. *ACS Chem Neurosci* **14**; 10.1021/acschemneuro.3c00384 (2023).

51. Brückner, G. *et al.* Cortical areas abundant in extracellular matrix chondroitin sulphate proteoglycans are less affected by cytoskeletal changes in Alzheimer's disease. *Neuroscience* **92,** 791–805; 10.1016/s0306-4522(99)00071-8 (1999).

52. Brady, D. R. & Mufson, E. J. Parvalbumin-immunoreactive neurons in the hippocampal formation of Alzheimer's diseased brain. *Neuroscience* **80,** 1113–1125; 10.1016/s0306-4522(97)00068-7 (1997).

53. Iritani, S., Niizato, K. & Emson, P. C. Relationship of calbindin D28K-immunoreactive cells and neuropathological changes in the hippocampal formation of Alzheimer's disease. *Neuropathology* **21,** 162–167; 10.1046/j.1440-1789.2001.00393.x (2001).

54. Mikkonen, M., Alafuzoff, I., Tapiola, T., Soininen, H. & Miettinen, R. Subfield- and layer-specific changes in parvalbumin, calretinin and calbindin-D28K immunoreactivity in the entorhinal cortex in Alzheimer's disease. *Neuroscience* **92,** 515–532; 10.1016/s0306-4522(99)00047-0 (1999).

55. Hartlage-Rübsamen, M. *et al.* Developmental expression and subcellular localization of glutaminyl cyclase in mouse brain. *Int J Dev Neurosci* **27,** 825–835; 10.1016/j.ijdevneu.2009.08.007 (2009).

56. Liu, J. *et al.* Microglial TMEM119 binds to amyloid-β to promote its clearance in an Aβ-depositing mouse model of Alzheimer's disease. *Immunity* **58,** 1830-1846.e7; 10.1016/j.immuni.2025.04.018 (2025).

57. Ardura-Fabregat, A. *et al.* Response of spatially defined microglia states with distinct chromatin accessibility in a mouse model of Alzheimer's disease. *Nat Neurosci* **28,** 1688–1703; 10.1038/s41593-025-02006-0 (2025).

58. Browne, P. & O'Cuinn, G. An evaluation of the role of a pyroglutamyl peptidase, a post-proline cleaving enzyme and a post-proline dipeptidyl amino peptidase, each purified from the soluble fraction of guinea-pig brain, in the degradation of thyroliberin in vitro. *Eur J Biochem* **137,** 75–87; 10.1111/j.1432-1033.1983.tb07797.x (1983).

59. Schilling, S. *et al.* On the seeding and oligomerization of pGlu-amyloid peptides (in vitro). *Biochemistry* **45,** 12393–12399; 10.1021/bi0612667 (2006).

60. Cabrera, E. *et al.* Aβ truncated species: Implications for brain clearance mechanisms and amyloid plaque deposition. *Biochim Biophys Acta Mol Basis Dis* **1864**; 10.1016/j.bbadis.2017.07.005 (2018).

61. Bouter, Y. *et al.* N-truncated amyloid β (Aβ) 4-42 forms stable aggregates and induces acute and long-lasting behavioral deficits. *Acta Neuropathol* **126,** 189–205; 10.1007/s00401-013-1129-2 (2013).

62. Hartlage-Rübsamen, M. *et al.* A glutaminyl cyclase-catalyzed α-synuclein modification identified in human synucleinopathies. *Acta Neuropathol* **142,** 399–421; 10.1007/s00401-021-02349-5 (2021).

63. Zhang, Y. *et al.* Glutaminyl cyclases, the potential targets of cancer and neurodegenerative diseases. *Eur J Pharmacol* **931,** 175178; 10.1016/j.ejphar.2022.175178 (2022).

64. Coimbra, J. R. M., Moreira, P. I., Santos, A. E. & Salvador, J. A. R. Therapeutic potential of glutaminyl cyclases: Current status and emerging trends. *Drug Discov Today*; 10.1016/j.drudis.2023.103644 (2023).

65. Logtenberg, M. E. W. *et al.* Glutaminyl cyclase is an enzymatic modifier of the CD47- SIRPα axis and a target for cancer immunotherapy. *Nat Med* **25,** 612–619; 10.1038/s41591-019-0356-z (2019).

66. Müller, K. *et al.* Combining daratumumab with CD47 blockade prolongs survival in preclinical models of pediatric T-ALL. *Blood* **140,** 45–57; 10.1182/blood.2021014485 (2022).

67. Dacon, C. *et al.* Protective antibodies target cryptic epitope unmasked by cleavage of malaria sporozoite protein. *Science* **387,** eadr0510; 10.1126/science.adr0510 (2025).

68. Wermelinger, L. S. *et al.* Fast analysis of low molecular mass compounds present in snake venom: identification of ten new pyroglutamate-containing peptides. *Rapid Commun Mass Spectrom* **19,** 1703–1708; 10.1002/rcm.1973 (2005).

69. Andrade-Silva, D., Nishiyama, M. Y., Stuginski, D. R., Zelanis, A. & Serrano, S. M. T. The distinct N-terminomes of Bothrops jararaca newborn and adult venoms. *Biochim Biophys Acta Proteins Proteom* **1869,** 140643; 10.1016/j.bbapap.2021.140643 (2021).

70. Awadé, A. C., Cleuziat, P., Gonzalès, T. & Robert-Baudouy, J. Pyrrolidone carboxyl peptidase (Pcp): an enzyme that removes pyroglutamic acid (pGlu) from pGlu-peptides and pGlu-proteins. *Proteins* **20,** 34–51; 10.1002/prot.340200106 (1994).

71. Dando, P. M., Fortunato, M., Strand, G. B., Smith, T. S. & Barrett, A. J. Pyroglutamyl-peptidase I: cloning, sequencing, and characterisation of the recombinant human enzyme. *Protein Expr Purif* **28**; 10.1016/s1046-5928(02)00632-0 (2003).

72. Hartlage-Rübsamen, M. *et al.* Immunohistochemical Evidence from APP-Transgenic Mice for Glutaminyl Cyclase as Drug Target to Diminish pE-Abeta Formation. *Molecules* **23,** 924; 10.3390/molecules23040924 (2018).

73. Bader, A. S. *et al.* Brain Region-Specific Differences in Amyloid-β Plaque Composition in 5XFAD Mice. *Life (Basel)* **13**; 10.3390/life13041053 (2023).

74. Talucci, I. *et al.* Aggregation-Dependent Epitope Sequence and Modification Fingerprints of Anti-Aβ Antibodies. *Elife* **14**; 10.7554/eLife.106156.1 (2025).

75. Oakley, H. *et al.* Intraneuronal beta-amyloid aggregates, neurodegeneration, and neuron loss in transgenic mice with five familial Alzheimer's disease mutations: potential factors in amyloid plaque formation. *J Neurosci* **26,** 10129–10140; 10.1523/JNEUROSCI.1202-06.2006 (2006).

76. Bluhm, A. *et al.* Immunohistochemical Demonstration of the pGlu79 α-Synuclein Fragment in Alzheimer's Disease and Its Tg2576 Mouse Model. *Biomolecules* **12,** 1006; 10.3390/biom12071006 (2022).

77. Beach, T. G. *et al.* Arizona Study of Aging and Neurodegenerative Disorders and Brain and Body Donation Program. *Neuropathology* **35,** 354–389; 10.1111/neup.12189 (2015).

78. Braak, H. & Braak, E. Neuropathological stageing of Alzheimer-related changes. *Acta Neuropathol* **82,** 239–259; 10.1007/BF00308809 (1991).

79. Mirra, S. S. *et al.* The Consortium to Establish a Registry for Alzheimer's Disease (CERAD). Part II. Standardization of the neuropathologic assessment of Alzheimer's disease. *Neurology* **41,** 479–486; 10.1212/wnl.41.4.479 (1991).

80. The National Institute on Aging & Reagan Institute Working Group on Diagnostic Criteria for the Neuropathological Assessment of Alzheimer's Disease. Consensus recommendations for the postmortem diagnosis of Alzheimer's disease. The National Institute on Aging, and Reagan Institute Working Group on Diagnostic Criteria for the Neuropathological Assessment of Alzheimer's Disease. *Neurobiol Aging* **18,** S1-2 (1997).

81. Faul, F., Erdfelder, E., Lang, A.-G. & Buchner, A. G*Power 3: a flexible statistical power analysis program for the social, behavioral, and biomedical sciences. *Behav Res Methods* **39,** 175–191; 10.3758/bf03193146 (2007).

82. Gattiker, A., Bienvenut, W. V., Bairoch, A. & Gasteiger, E. FindPept, a tool to identify unmatched masses in peptide mass fingerprinting protein identification. *Proteomics* **2,** 1435–1444; 10.1002/1615-9861(200210)2:10<1435::AID-PROT1435>3.0.CO;2-9 (2002).

83. Gnoth, K. *et al.* Targeting isoaspartate-modified Aβ rescues behavioral deficits in transgenic mice with Alzheimer's disease-like pathology. *Alzheimers Res Ther* **12,** 149; 10.1186/s13195-020-00719-x (2020).

84. Wirths, O. *et al.* Amino-terminally elongated Aβ peptides are generated by the secreted metalloprotease ADAMTS4 and deposit in a subset of Alzheimer's disease brains. *Neuropathol Appl Neurobiol* **50,** e12991; 10.1111/nan.12991 (2024).

85. Klafki, H.-W. *et al.* Detection and quantification of Aβ-3-40 (APP669-711) in cerebrospinal fluid. *J Neurochem* **160,** 578–589; 10.1111/jnc.15571 (2022).

86. Piechotta, A. *et al.* Structural and functional analyses of pyroglutamate-amyloid-β-specific antibodies as a basis for Alzheimer immunotherapy. *J Biol Chem* **292,** 12713–12724; 10.1074/jbc.M117.777839 (2017).

87. Köppen, J. *et al.* Amyloid-Beta Peptides Trigger Aggregation of Alpha-Synuclein In Vitro. *Molecules* **25,** 580; 10.3390/molecules25030580 (2020).

88. Koressaar, T. & Remm, M. Enhancements and modifications of primer design program Primer3. *Bioinformatics* **23,** 1289–1291; 10.1093/bioinformatics/btm091 (2007).

89. Kõressaar, T. *et al.* Primer3_masker: integrating masking of template sequence with primer design software. *Bioinformatics* **34,** 1937–1938; 10.1093/bioinformatics/bty036 (2018).

90. Untergasser, A. *et al.* Primer3-new capabilities and interfaces. *Nucleic Acids Res* **40,** e115; 10.1093/nar/gks596 (2012).

91. Ye, J. *et al.* Primer-BLAST: a tool to design target-specific primers for polymerase chain reaction. *BMC Bioinformatics* **13,** 134; 10.1186/1471-2105-13-134 (2012).

92. Bluhm, A. *et al.* Monomers, Dimers, and Oligomers of Pyroglutamate-Modified α-Synuclein Fragments Exhibit Distinct Biophysical Characteristics. *ACS Chem Neurosci* **16,** 1919–1936; 10.1021/acschemneuro.5c00106 (2025).

93. Oberstadt, M. *et al.* TDP-43 self-interaction is modulated by redox-active compounds Auranofin, Chelerythrine and Riluzole. *Sci Rep* **8,** 2248; 10.1038/s41598-018-20565-0 (2018).

94. Thal, D. R., Walter, J., Saido, T. C. & Fändrich, M. Neuropathology and biochemistry of Aβ and its aggregates in Alzheimer's disease. *Acta Neuropathol* **129**; 10.1007/s00401-014-1375-y (2015).

95. Thal, D. R., Rüb, U., Orantes, M. & Braak, H. Phases of Abeta-deposition in the human brain and its relevance for the development of AD. *Neurology* **58,** 1791–1800; 10.1212/wnl.58.12.1791 (2002).

96. Beach, T. G. *et al.* Unified staging system for Lewy body disorders: correlation with nigrostriatal degeneration, cognitive impairment and motor dysfunction. *Acta Neuropathol* **117,** 613–634; 10.1007/s00401-009-0538-8 (2009).

Supplementary Files

This is a list of supplementary files associated with this preprint. Click to download.

- SupplementaryMaterialRTqPCR.docx